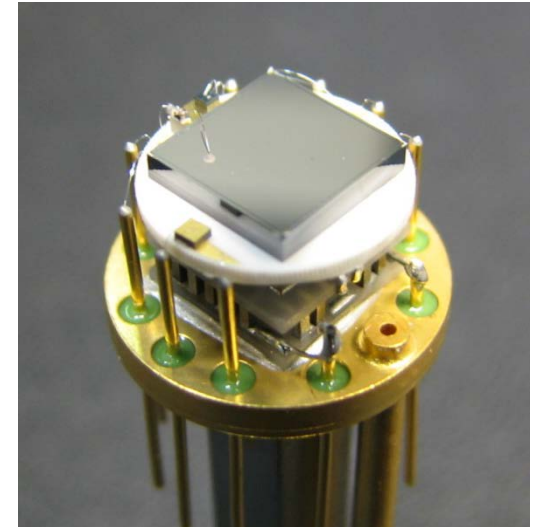
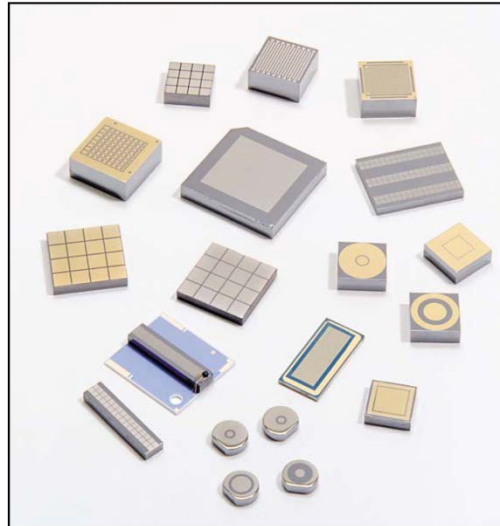
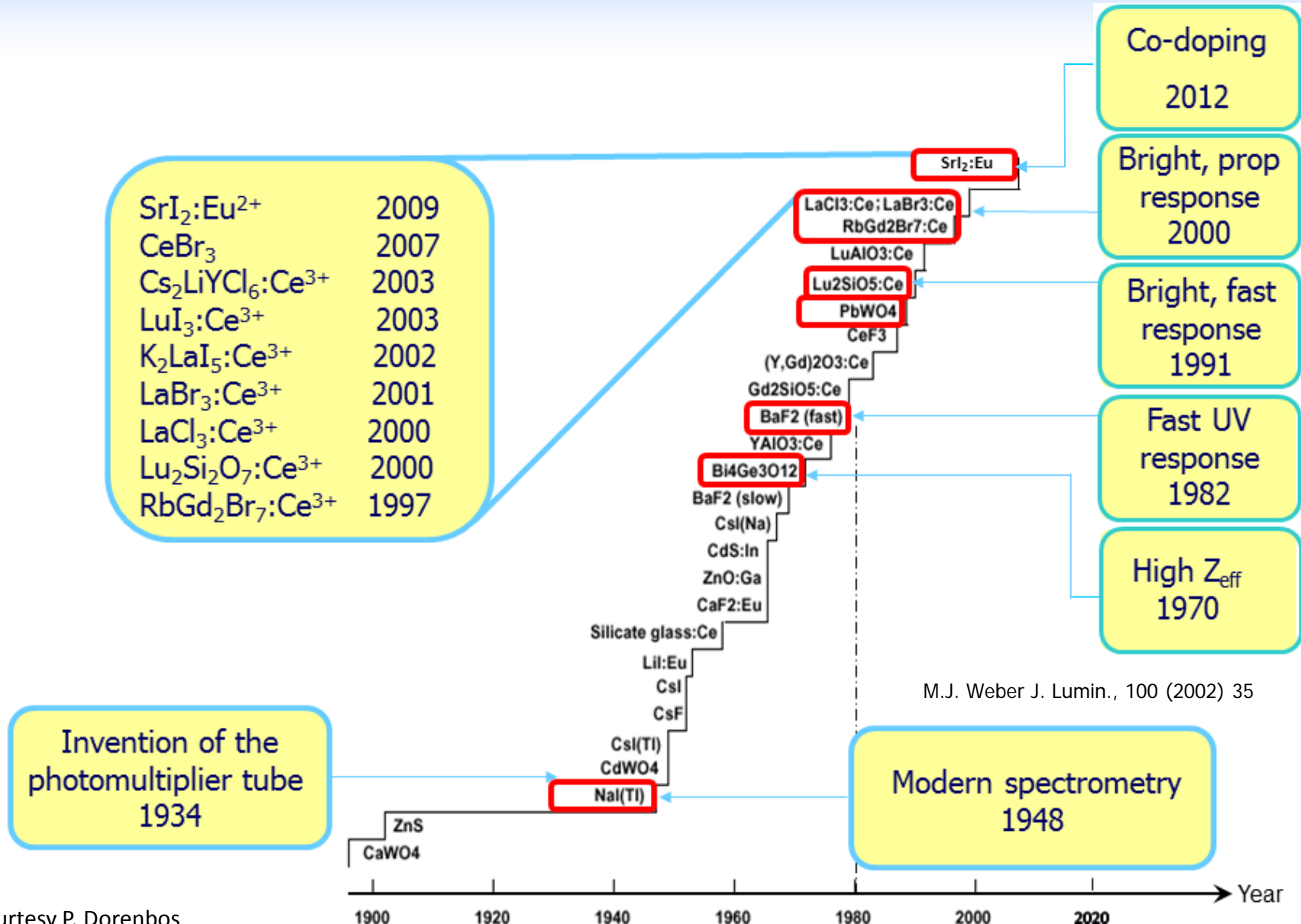


The quest for optimized sensor materials

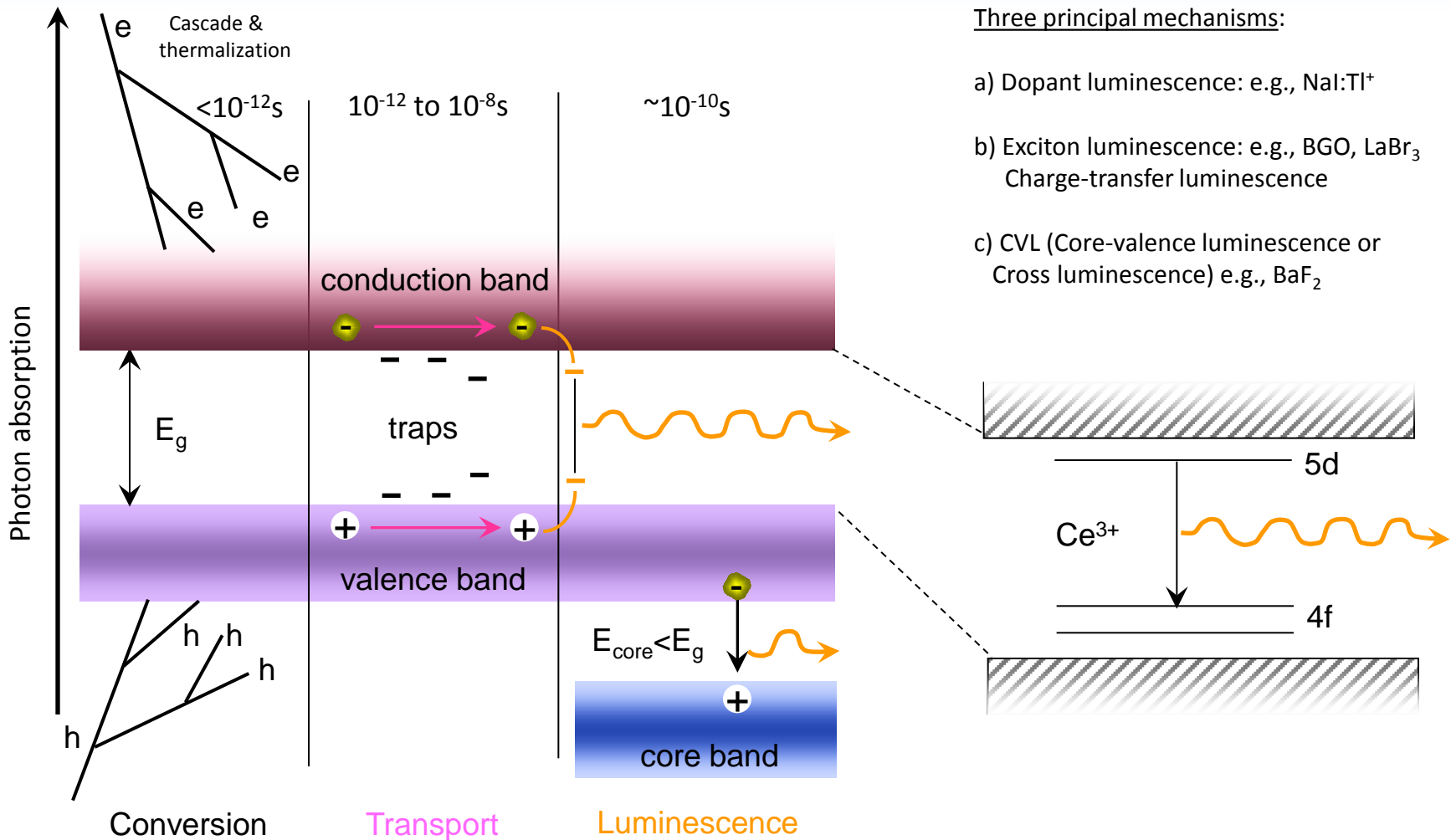


Alan Owens
European Space Agency
Noordwijk, The Netherlands

- A brief history
- Semiconductor and scintillator materials
- Detection systems
- Performance limitations
- Improving performance
- New detection techniques



M.J. Weber J. Lumin., 100 (2002) 35



M. Nikl, *Scintillation detectors for X-rays*, Meas. Sci. Technol., 17 (2006) R37.

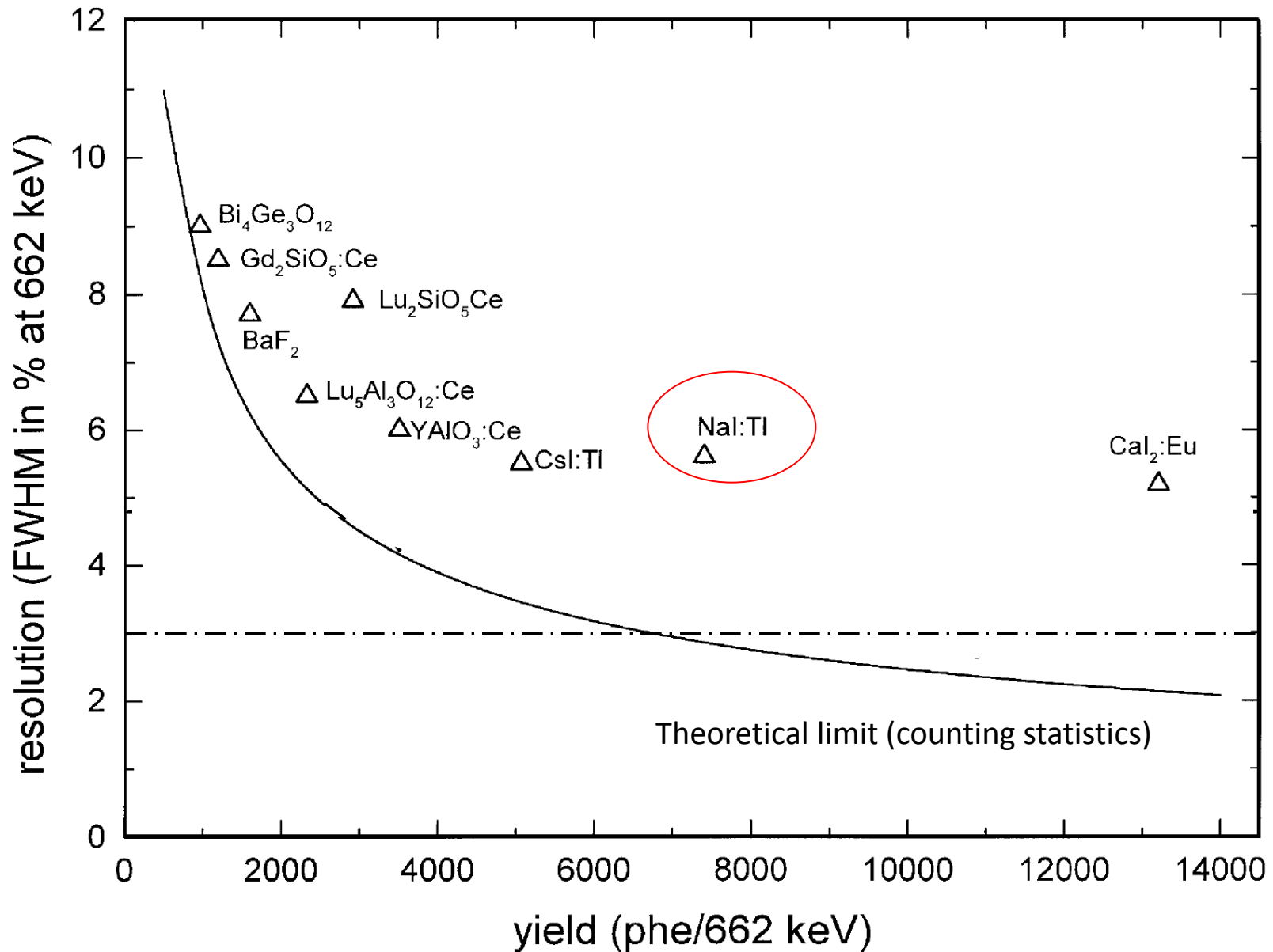
Advantages

- Simple
- Essentially passive
- Radiation hard
- Can be grown in large sizes \Rightarrow area detectors
- Make good gamma-ray detectors \Rightarrow volume

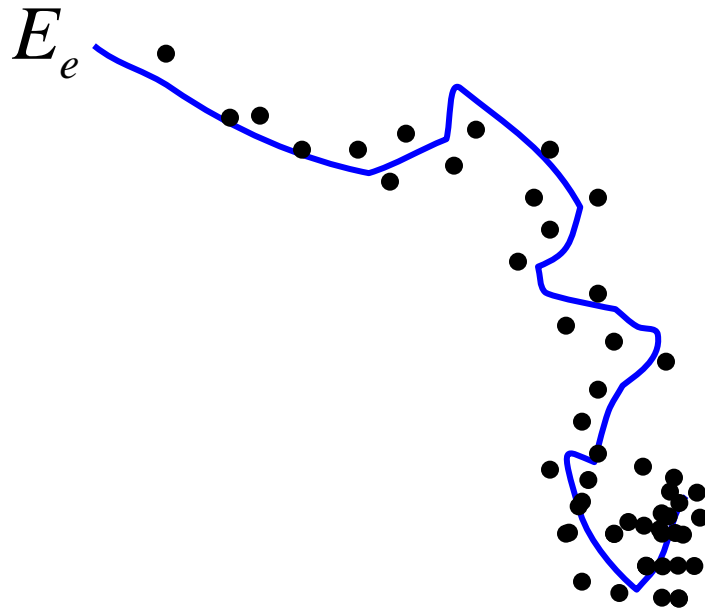
Disadvantages

- Non-proportional response
- Limited potential in spatially resolved spectroscopy (Anger cameras?)
- New generation of high resolution scintillators are expensive
- Generally hygroscopic (especially inorganic crystals)
- Requires separate read-out device

But.....



1) R_{stat} - creation of the ionization track



$$N_{eh} = \frac{E}{W_{eh}} = \frac{E_{\gamma}}{\beta E_g}$$

$$\left. \begin{array}{l} \beta \approx 2.5 \\ E_g = 5.8 \text{ eV} \end{array} \right\} \Rightarrow N_{eh} = 69,000 \text{ /MeV}$$

$$\Rightarrow \sigma = \sqrt{N_{eh}}$$

For a 662 keV energy deposition, $\Delta E/E = 1\%$

$R_{\text{stat}} \Rightarrow$ Does not limit resolution

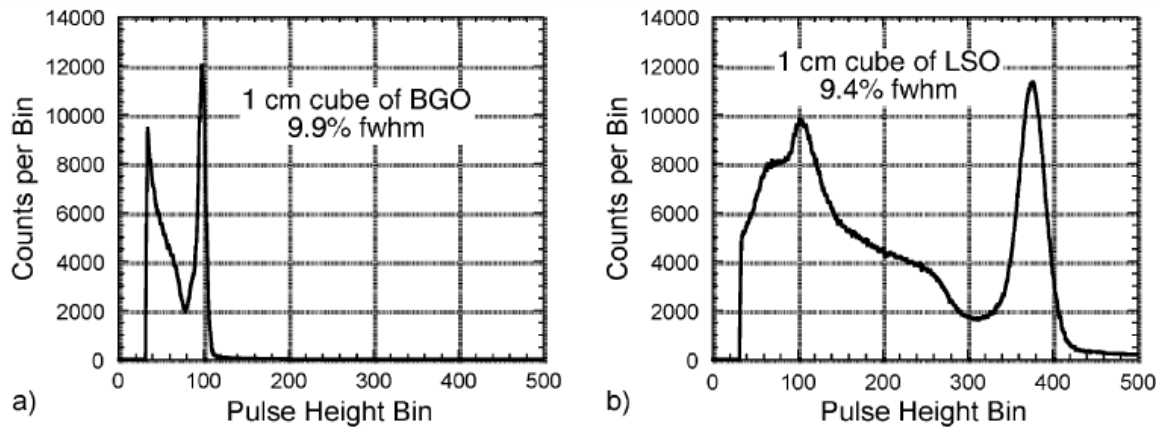


Fig. 1. Pulse height spectra under 662 keV gamma ray excitation. (a) 1 cm cube of BGO. (b) 1 cm cube of LSO.

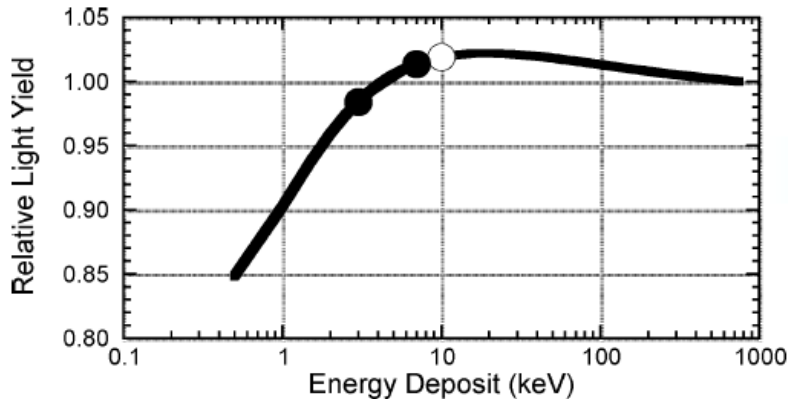


Fig. 2. Photon response curve for a hypothetical scintillator. The y -axis plots the relative light yield (the luminous efficiency, in photons per MeV, normalized to the value at 662 keV) as a function of the energy of the photon that excited it, which is plotted on the x -axis. Deviations from a horizontal line are “non-proportionality,” meaning that the luminous efficiency depends on the incident energy.

$E_{\gamma 1} = 662 \text{ keV} \rightarrow$ collection of n secondary electrons with energies $E_1, E_2, \dots, E_i, \dots, E_n$. Photon yield $Y(E_i)$ due to electron i depends on electron energy.

$E_{\gamma 2} = 662 \text{ keV} \rightarrow$ another collection of m secondary electrons with energies $E_1, E_2, \dots, E_j, \dots, E_m$.

$$Y_{\gamma 1} = \sum_{i=1}^n Y(E_i) \neq Y_{\gamma 2} = \sum_{j=1}^m Y(E_j)$$

From Moses, IEEE Trans. Nucl. Sci., **55** (2008) 1049-1053

- Statistics in the number of detected photons, N_{stat}
- Non-proportional response of the scintillator, N_{np}
- Inhomogeneities in the crystal, light reflection, or photocathode, N_{inh}
- Contributions from the statistics in the gain of the PMT or electronic noise in (A)PDs, N_{det}

$$R^2 = R_{stat}^2 + R_{np}^2 + R_{inh}^2 + R_{det}^2$$

7.8%

2.0%

7.0%

1.0%

3.0%

Contributions at 662 keV for a 1 inch RCC NaI(Tl) xtal + PMT

Produce a large volume gamma-ray detector with:

- High γ -ray detection efficiency in the MeV region, $\varepsilon_p > 14\%$ @ 1 MeV

Achieve through use of high density materials (i.e., $> 5 \text{ g cm}^{-3}$)

- High energy resolution better than 3% FWHM @ 662 keV

Achieve using scintillation materials with high light output ($> 50,000 \text{ ph/MeV}$) – require low light non-proportionality, low readout noise ($< 20 \text{ phe rms}$)

- Environmentally robust

Hardness $> 2 \text{ Mho}$, Radiation tolerance $> 1 \text{ Mrad}$, 10^4 Gy , low activation susceptibility ($< 3 \text{ ct cm}^{-3} \text{ s}^{-1}$),

Achieve using low phosphorescence inorganic scintillators, radiation damage mitigation via annealing possibility *via* thermal or optical bleaching means

- Inert

Room or elevated temperature operation (-10°C to $+50^\circ\text{C}$), no special EMC, cleanliness or handling requirements, no moving parts

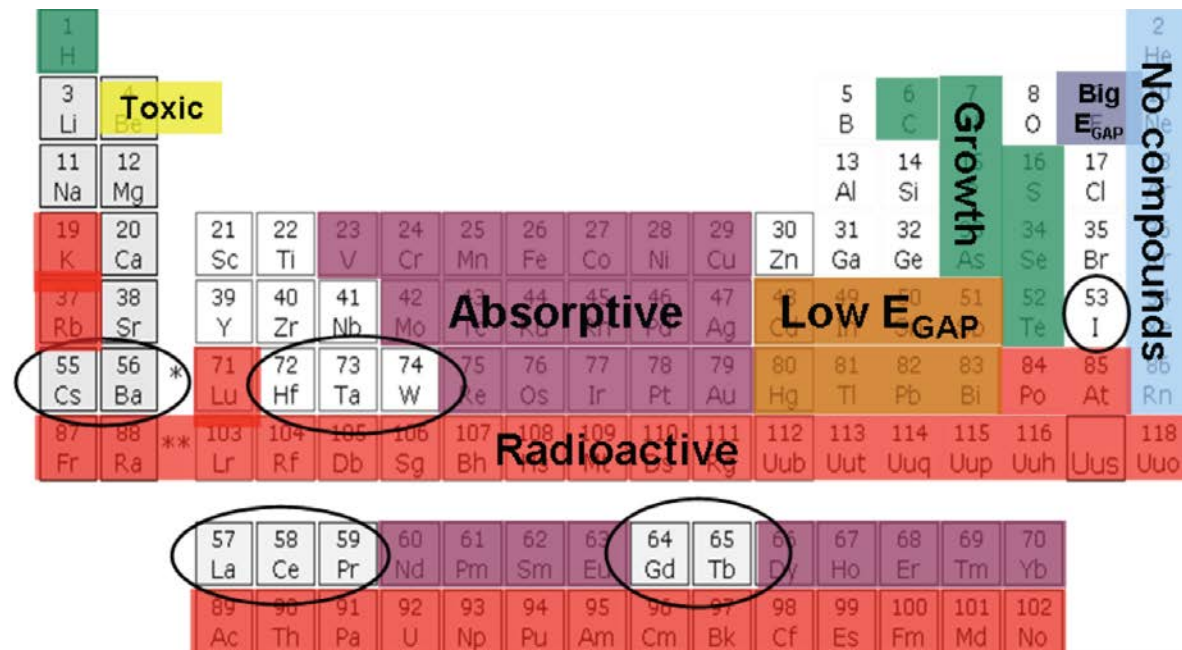
- Minimally resourced

No services (e.g., cooling, vacuum, calibration sources, radiation or magnetic shielding), no maintenance, 4 kg, 4W, 1 L – above all simple

Inferred from the BepiColombo SCI-RD

Goal - scintillator with 3% or better energy resolution at 662 keV. The selection of candidate materials for gamma ray spectroscopy is relatively straightforward since they must be formed out of elements (shown encircled below) which are,

- 1) high- Z_{eff} (equivalent or higher than LaBr_3)
- 2) that are not radioactive,
- 3) that are not optically absorptive,
- 4) have a band gap that $1\text{eV} < \epsilon_g < 10\text{eV}$, (good statistics)
- 5) focus on binary alkaline earth halides (high light outputs)
- 6) it must be possible to grow the candidate material in stable form (low ΔG_f - Gibbs free energy of formation)



Compound	Light Yield, Photons/MeV	Peak emission (nm)	Decay time (ns)	nPr 1- σ_{PR}	Figure of merit
PbWO ₄	250	590	98	0.93	
Bi ₄ Ge ₃ O ₁₂ (BGO)	8000	480	300	0.91	
BaF ₂	10000	310	620	0.97	
Lu ₂ SiO ₅ :Ce (LSO)	30000	420	40	0.78	
Lu _{1.8} Y _{0.2} SiO ₅ :Ce (LYSO)	34000	397	41	0.89	
NaI:Tl	45000	415	230	0.85	
CsI:Tl ⁺	56000	550	980	0.86	
LaCl:Ce ³⁺	48000	350	28	0.94	98
LaBr ₃ :Ce ³⁺	75000	380	30	0.95	111

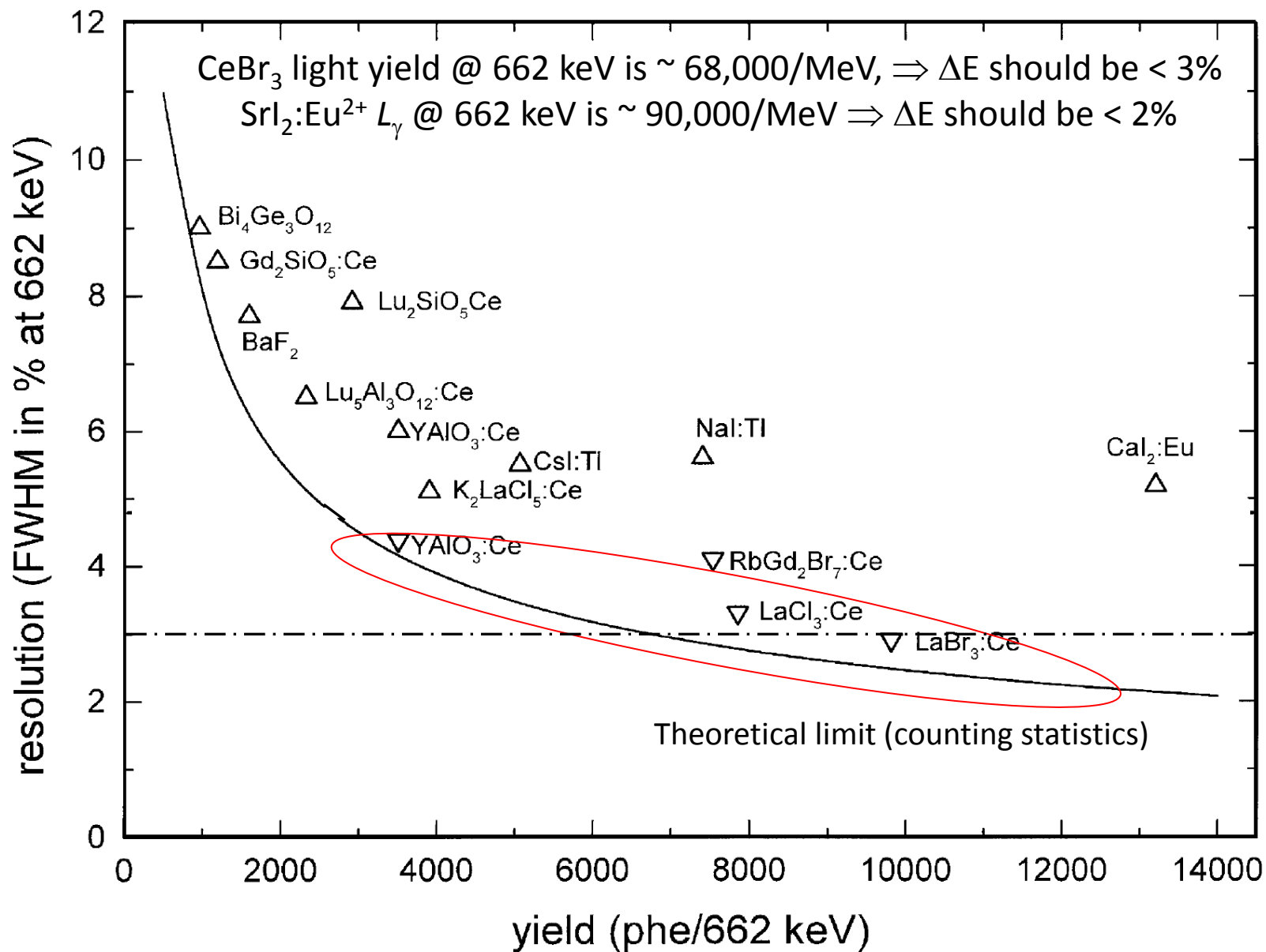
Figure of merit based on a modified form of minimum sensitivity in the presence of a background equations given in Cooper and Chupp.

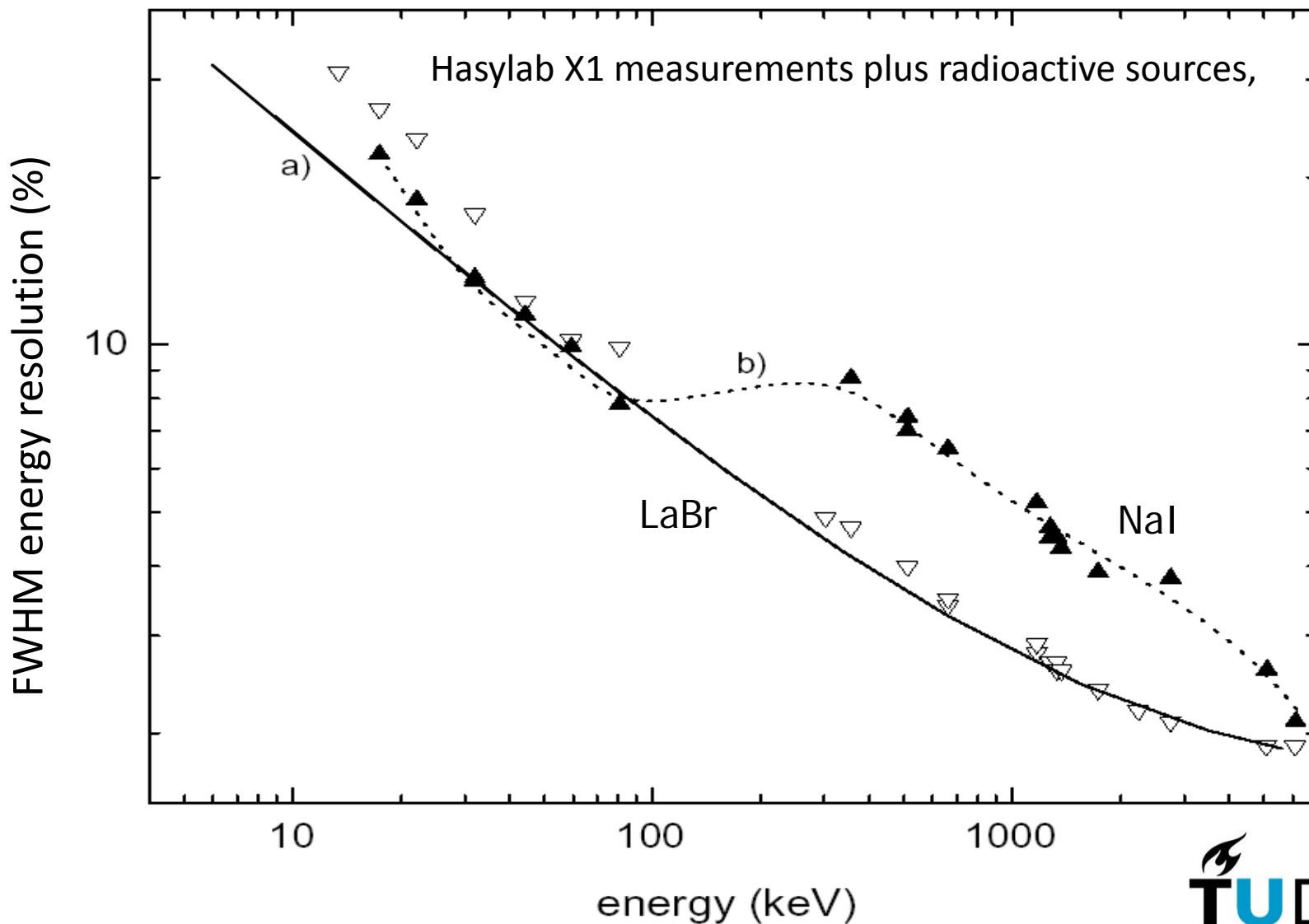
Does not take into account nPr

J.A. Cooper, "Factors Determining the Ultimate Sensitivity of Ge(Li) Gamma-Ray Spectrometers", Nucl. Instr. and Meth., **82** (1970) 273.

E.L. Chupp, "Gamma Ray Astronomy (Nuclear Transition Region)", D. Reidel Publishing Company, Dordrecht, Holland (1976)

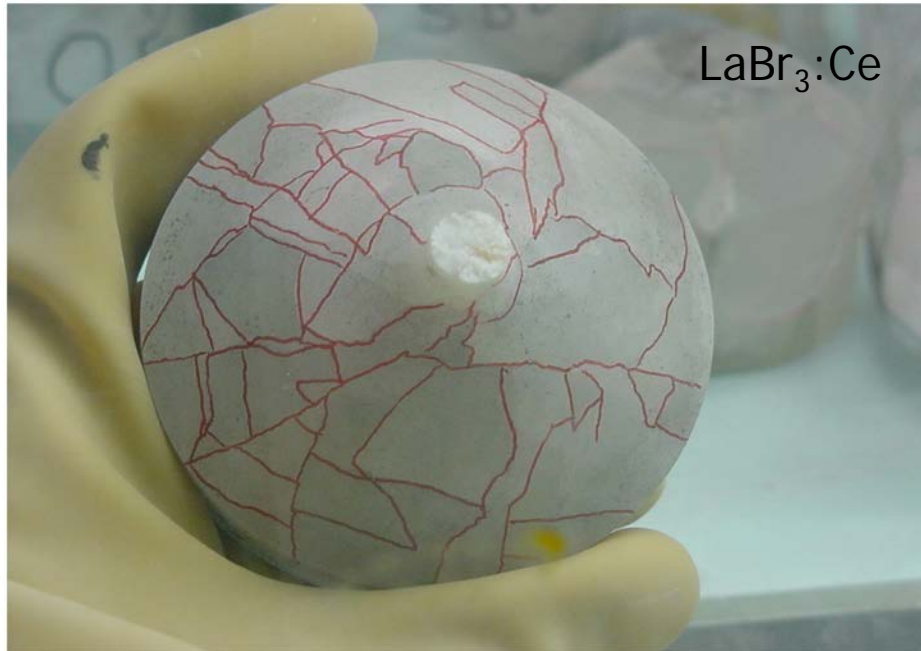
The cerium doped halides





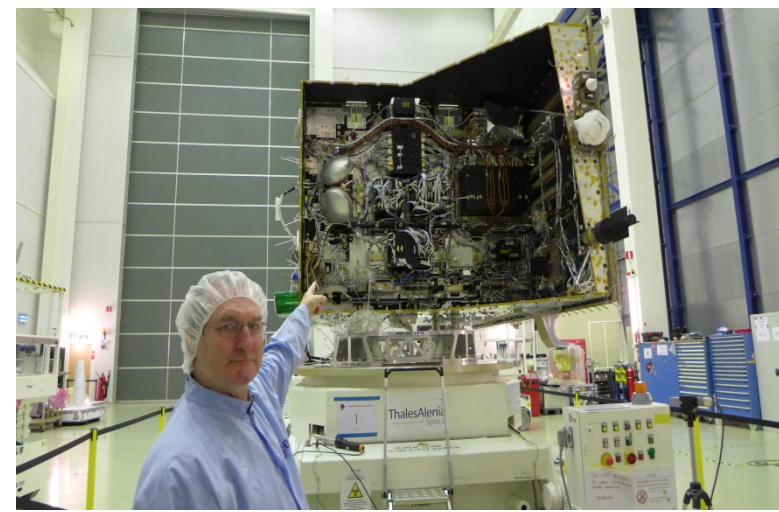
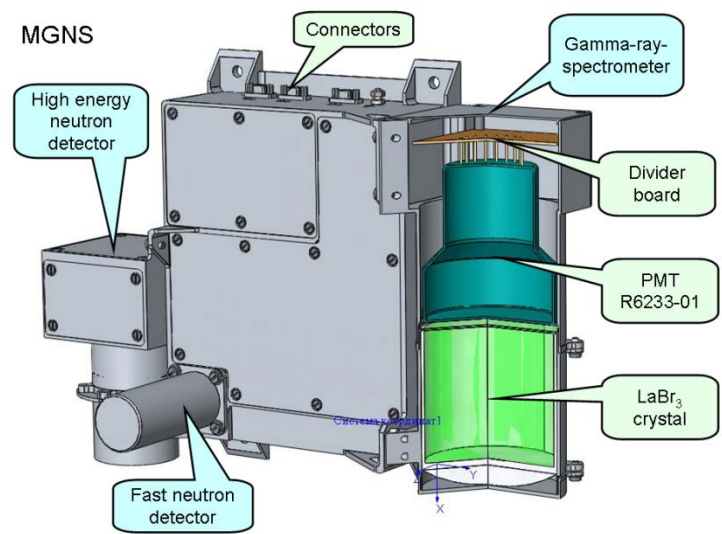
Current project crystal growth capabilities

Crystal growth at St Gobain, France/Hellma Materials, Jena, Germany

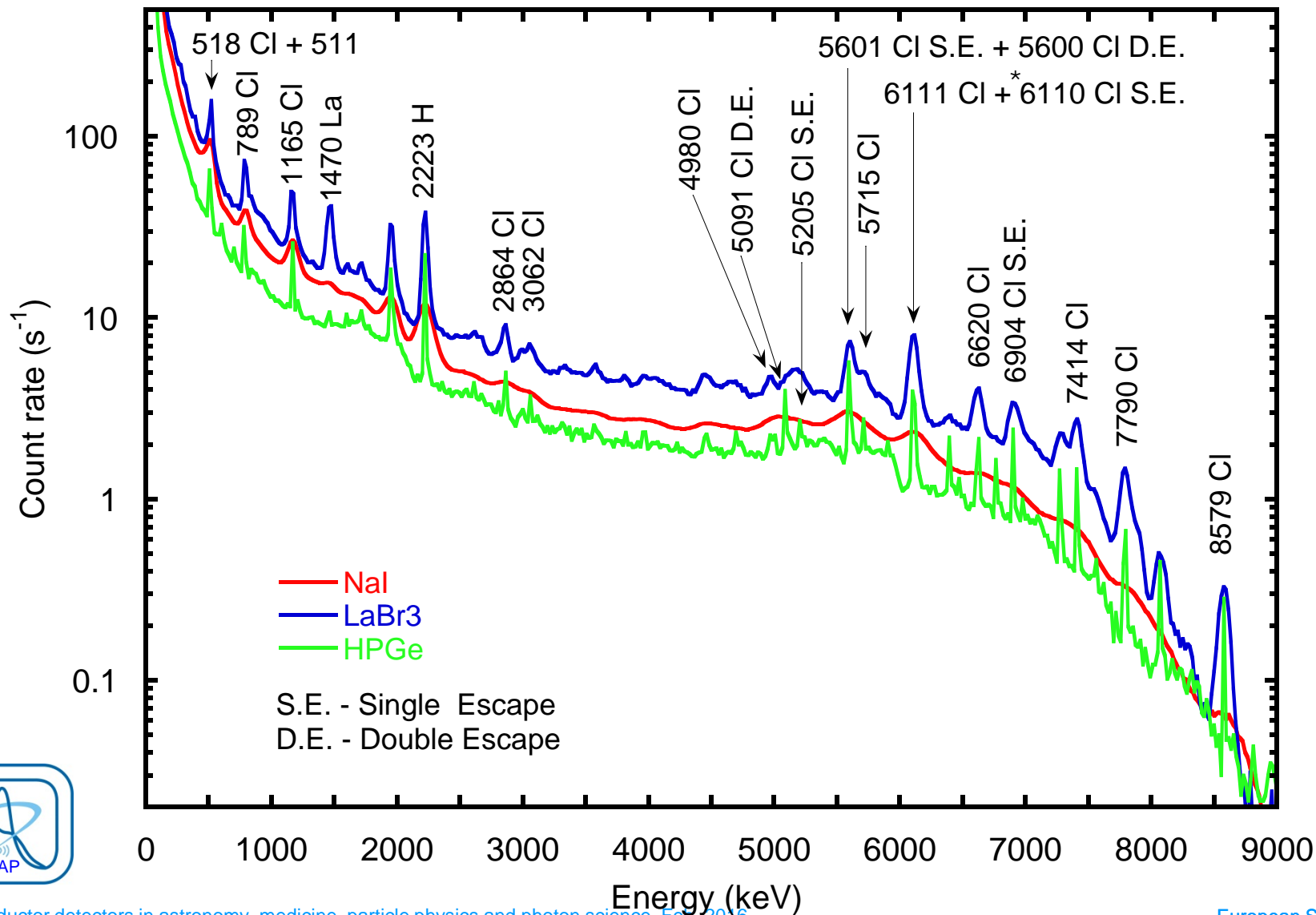


esa Output of the XBr_3 scintillator development program

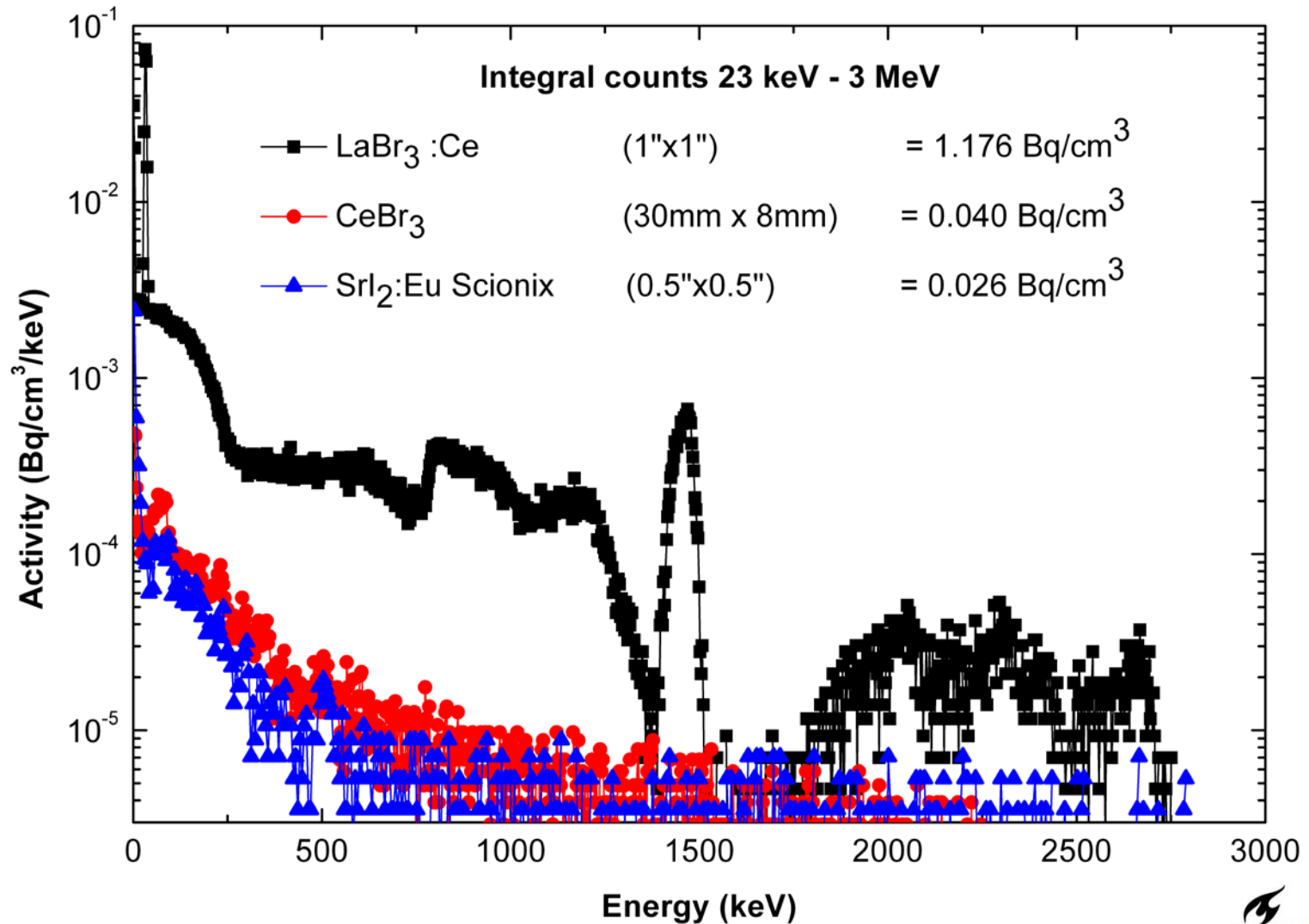
$LaBr_3$ (10% Ce) gives the best energy resolution. For a 3 inch RCC, ΔE is 3% FWHM at 662 keV. The intrinsic background level is 1 Bq cm^{-3} . Two 2 inch xtals were flown onboard Phobos Grunt. The three inch xtal on BepiColombo has been swapped-out with a 3 inch 4.5% $CeBr_3$ xtal during final integration



3x3 inch LaBr₃, 3x3 inch NaI(Tl), 6.5 cm HPGe, uniform illumination



Measured in lead castle at TU Delft with low ^{40}K PMT. LaBr_3 used as benchmark



Compound	Light Yield, Photons/MeV	Peak emission (nm)	Decay time (ns)	nPr $1-\sigma_{PR}$	Figure of merit
LaCl:Ce ³⁺	48000	350	28	0.94	98
LaBr ₃ :Ce ³⁺	75000	380	30	0.95	111
Cs ₂ LiLaBr ₆ :Ce (CLLB)	60000	410	270	0.95?	169
Gd ₃ Sc ₂ Al ₃ O ₁₂ :Ce (GYGAG)	48000	570	100	0.99?	827
CeBr ₃	68000	370	17	0.93	596
SrI ₂ :Eu ²⁺	90000	430	1200	0.98	1045

Figure of merit based on a modified form of minimum sensitivity in the presence of a background equations given in Cooper and Chupp.

Does not take into account nPr

J.A. Cooper, "Factors Determining the Ultimate Sensitivity of Ge(Li) Gamma-Ray Spectrometers", Nucl. Instr. and Meth., **82** (1970) 273.

E.L. Chupp, "Gamma Ray Astronomy (Nuclear Transition Region)", D. Reidel Publishing Company, Dordrecht, Holland (1976)

Given that Ce^{3+} , Pr^{3+} and Eu^{2+} are the current activator workhorse. The choice of scintillator is driven by aspects of the 5d-4f decay scheme.

⇒ For Ce doping, the light yield limit of 100-130 ph/keV and decay time limit of 15-17 ns has been approached

⇒ For Pr doping, a reduction in decay time from 20 ns-10 ns is still possible

⇒ For both Pr and Eu larger light yields are still possible

Condition for room temperature stable 5d-4f emission:

$E_{5d} < E_{cb} - 0.5 \text{ eV}$, otherwise trapping occurs

$E_{4f} > E_{vb} + 0.5 \text{ eV}$ otherwise quenching occurs

* For Ce^{3+} doping the optimum material has a light yield of 100-130 ph/keV a BG of 3-4 eV and a decay time of 20 ns

* For Pr^{3+} doped scintillators, the optimum material has a LY of 65-80 ph/keV and a bandgap 5-6 eV and a decay time of 10 ns

* For Eu^{2+} doped scintillators, the optimum material has a LY of 105-140 ph/keV and a bandgap 2.8-3.8 eV

- Sr co-doping of LaBr_3 has achieved a ΔE of 2% at 662 keV
- Sr co-doping of CeBr_3 has achieved a ΔE of 3% at 662 keV

Advantages

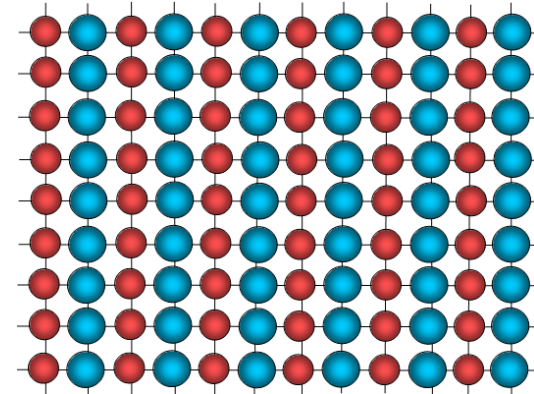
- Wide variety of compounds available
- Compounds can be selected for specific environments
- Materials can be engineered for specific applications
- Electronics can be integrated – e.g. DEPFET
- Very good for spatially resolved spectroscopy applications

Disadvantages

- Requires hyperpure material - expensive
- Usually requires cooling for best performance
- Difficult to grow in large sizes - not good for area detectors
- Radiation damage issues

Follow the Hume-Rothery rules

- The **atomic radii** of the different atoms involved must **differ by less than 15%**
- The components must have the **same crystal structure**
- The species must have **similar valences**
- The components must **have similar electronegativities**



Rational

- Atomic radii must be similar because if substituted atom is too large, considerable strain will develop in crystal lattice
- The components must have similar crystal structure if solubility is to occur over all proportions, e.g., the CdTe-ZnTe system. However, this is less important if small proportions of solute being added - such as in the doping of semiconductors.
- Similar valences and electronegativities indicates that components have similar bonding properties.

Mooser-Pearson laws

Materials will show semiconducting properties if they obey the following rules:

- 1) The bonds are predominantly covalent.
- 2) The bonds are formed by a process of electron sharing which leads to completely filled **s** and **p** sub-shells on all atoms in elemental semiconductors. For compound semiconductors, the condition has to apply for each constituent element.
- 3) The presence of vacant “metallic” orbital’s on some atoms in a compound will not prevent semiconductivity provided that these atoms are not bonded together.
- 4) The bonds form a continuous array in one, two or three dimensions throughout the crystal.

Elements from groups IV to group VII will satisfy conditions 1 and 2. Compounds which follow the second condition can be represented by the following expression †.

$$n_e / n_a + b = 8$$

Here, n_e is the number of valence electrons per molecule, n_a is the number of group IV to VII atoms per molecule and b is the average number of covalent bonds formed by one of these atoms with other atoms of groups IV to VII. Thus, for GaAs, $n_e=8$, $n_a=1$ and $b=0$ – which equals 8.

Bottom line for binaries, the group numbers should add up to 8 – i.e., group I-VII, III-V, IV-IV, II-VI and I-VII

†Equivalent to the 8-N rule

E. Mooser, W.B.Pearson, “*The Chemical Bond in Semiconductors*”, J. Electron., Vol.1 (1956) pp. 629-645

Deriving new semiconductors



- binary — IV-IV — SiGe, SiC
- binary — III-V — InP, GaAs, GaN
- binary — II-VI — HgTe, CdSe, ZnS
- binary — I-VII — AgCl, AgBr, CuCl
- ternary — all — HgCdTe, AlGaAs
- quaternary — all — InGaAsP, InGaAlP

hydrogen 1 H 1.0079	beryllium 4 Be																	helium 2 He 4.0026
lithium 3 Li 6.941																		neon 10 Ne 20.180
sodium 11 Na 22.990	magnesium 12 Mg 24.305																	argon 18 Ar 39.948
potassium 19 K 39.098	calcium 20 Ca 40.078	scandium 21 Sc 44.956	titanium 22 Ti 47.867	vanadium 23 V 50.942	chromium 24 Cr 51.996	manganese 25 Mn 54.938	iron 26 Fe 55.845	cobalt 27 Co 58.933	nickel 28 Ni 58.693	copper 29 Cu 63.5	zinc 30 Zn 65.38	gallium 31 Ga 69.7	germanium 32 Ge 72.6	arsenic 33 As 74.9	selecnium 34 Se 79.0	bromine 35 Br 79.9	krypton 36 Kr 83.80	
rubidium 37 Rb 85.468	strontium 38 Sr 87.62	yttrium 39 Y 88.906	zirconium 40 Zr 91.224	niobium 41 Nb 92.906	niobium 42 Mo 95.94	technetium 43 Tc [98]	ruthenium 44 Ru 101.07	rhodium 45 Rh 102.91	palladium 46 Pd 106.42	silver 47 Ag 107.9	cadmium 48 Cd 112.4	indium 49 In 114.8	tin 50 Sn 118.7	antimony 51 Sb 121.8	tellurium 52 Te 127.6	iodine 53 I 126.9	xenon 54 Xe 131.29	
cesium 55 Cs 132.91	barium 56 Ba 137.21	* 57-70	lanthanum 57 La 138.91	hafnium 71 Hf 178.49	tantalum 72 Ta 180.95	wolfram 73 W 183.84	reuterium 74 Re 186.21	osmium 75 Os 190.23	iridium 76 Ir 192.22	platinum 77 Pt 195.08	gold 78 Au 197.0	mercury 79 Hg 200.6	thallium 80 Tl 204.4	lead 81 Pb 207.2	bismuth 82 Bi 209.0	polonium 83 Po 210.0	astatine 84 At [210]	radon 86 Rn [222]
francium 87 Fr [223]	radium 88 Ra [226]	* 89-102	actinium 89 Ac [227]	rutherfordium 103 Rf [261]	bohrium 104 Bh [264]	hassium 105 Hs [268]	meitnerium 106 Mt [268]	unnilium 107 Uun [271]	unnilium 108 Uun [271]	ununium 109 Uun [273]	ununium 110 Uun [273]	ununium 111 Uun [277]	ununium 112 Uun [277]	ununium 113 Uun [289]	ununium 114 Uun [289]			

* Lanthanide series

lanthanum 57 La 138.91	cerium 58 Ce 140.12	praseodymium 59 Pr 140.91	neodymium 60 Nd 144.24	promethium 61 Pm [145]	samarium 62 Sm 150.36	europium 63 Eu 151.96	gadolinium 64 Gd 157.25	terbium 65 Tb 158.93	dysprosium 66 Dy 162.50	holmium 67 Ho 164.93	erbium 68 Er 167.26	thulium 69 Tm 168.93	ytterbium 70 Yb 173.04
---------------------------------	------------------------------	------------------------------------	---------------------------------	---------------------------------	--------------------------------	--------------------------------	----------------------------------	-------------------------------	----------------------------------	-------------------------------	------------------------------	-------------------------------	---------------------------------

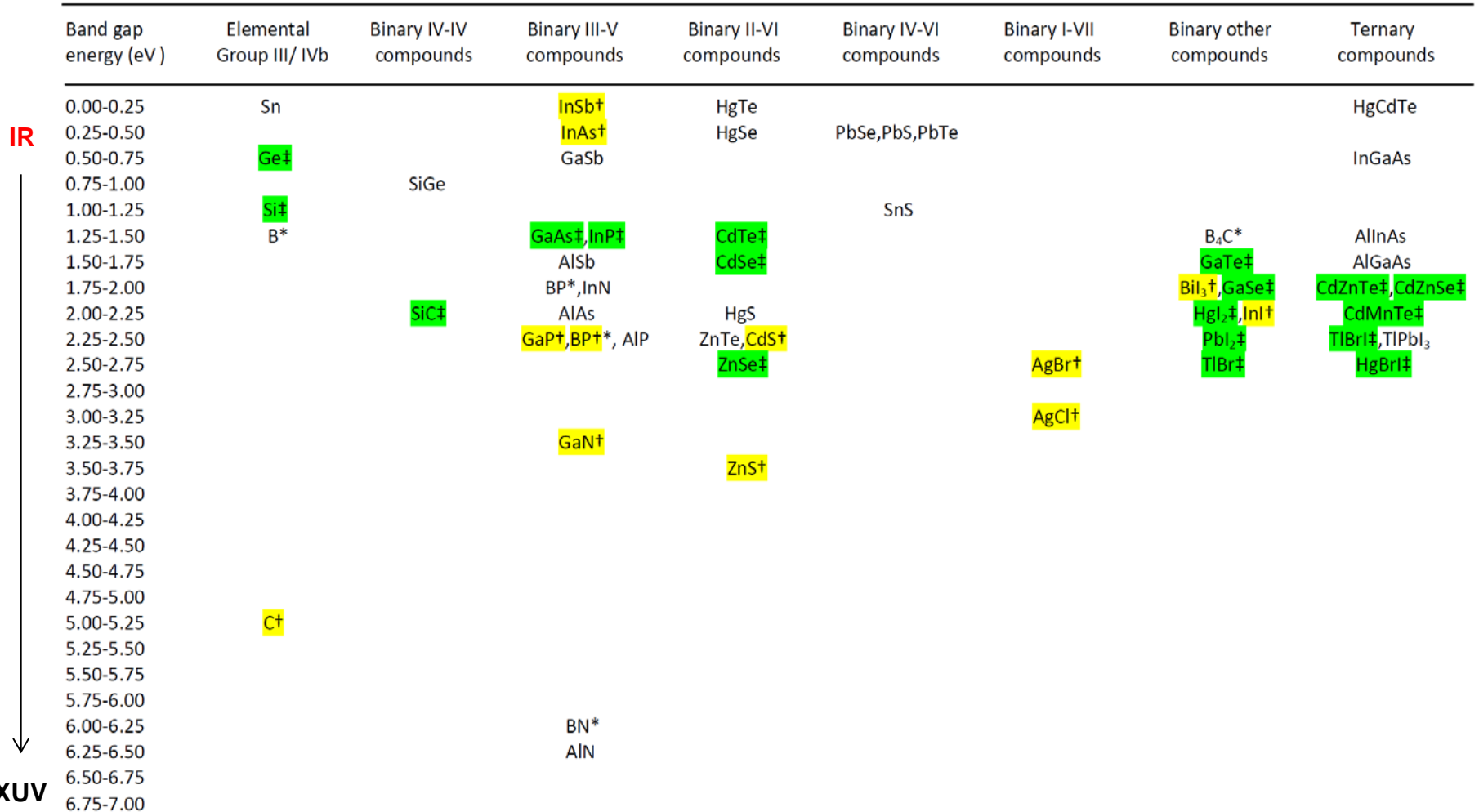
** Actinide series

actinium 89 Ac [227]	thorium 90 Th 232.04	protactinium 91 Pa 231.04	uranium 92 U 238.03	neptunium 93 Np [237]	plutonium 94 Pu [244]	americium 95 Am [243]	curium 96 Cm [247]	berkelium 97 Bk [247]	californium 98 Cf [251]	einsteinium 99 Es [252]	fermium 100 Fm [257]	mendeleevium 101 Md [258]	nobelium 102 No [259]
-------------------------------	-------------------------------	------------------------------------	------------------------------	--------------------------------	--------------------------------	--------------------------------	-----------------------------	--------------------------------	----------------------------------	----------------------------------	-------------------------------	------------------------------------	--------------------------------

Elemental semiconductors essentially limited to C, Si and Ge

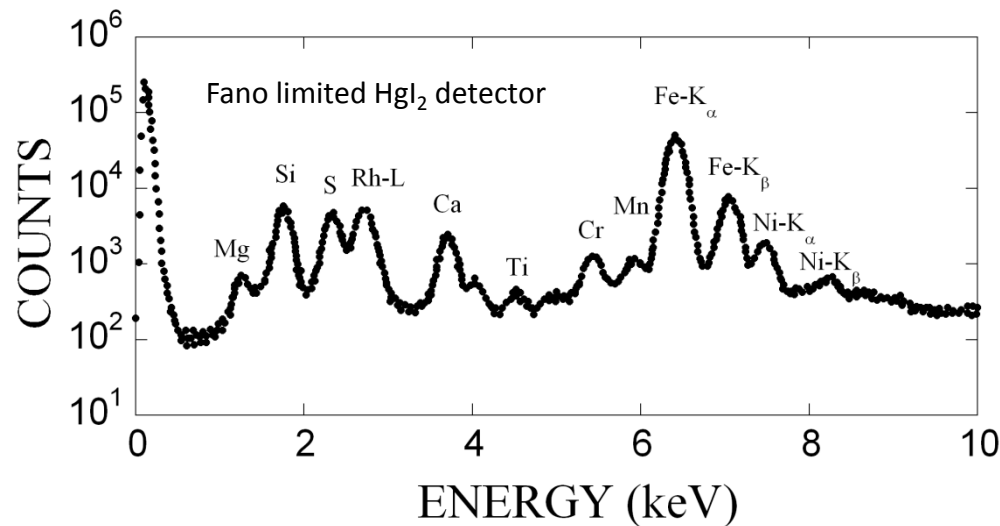
What has been looked at?

Compound semiconductor material listed by group and in order of increasing band-gap energy ranging from near IR to XUV wavelengths

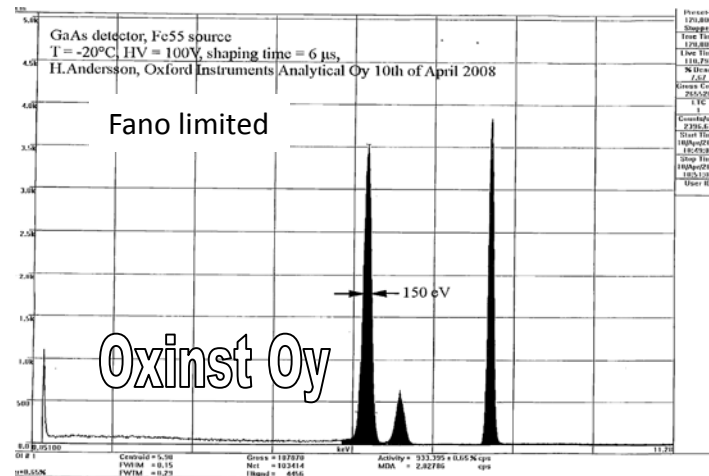


† Compounds which have shown a response to energetic radiation. ‡ Materials for which spectroscopic measurements (i.e. $\Delta E/E > 1$) have been made at X-ray wavelengths. * Investigated for n detection.

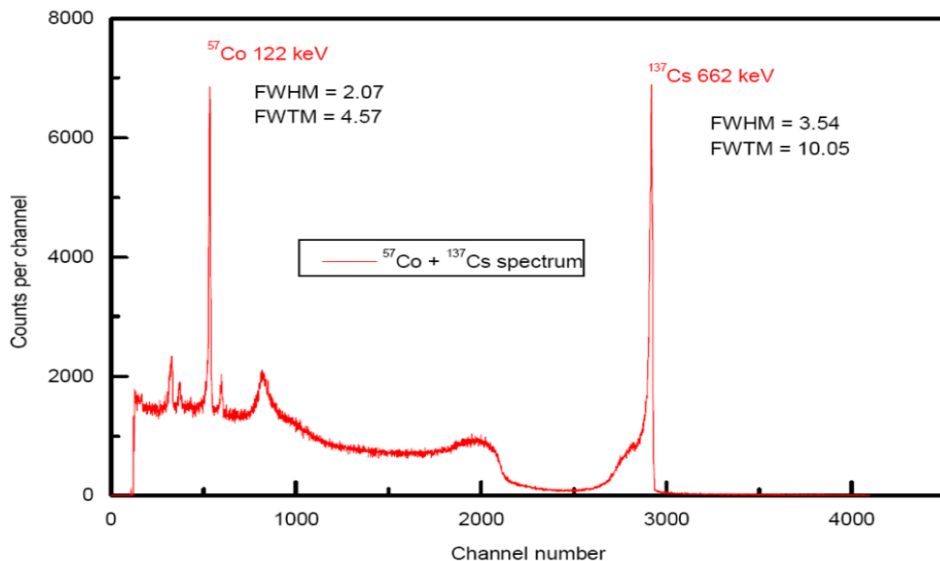
Some of the best spectroscopic results



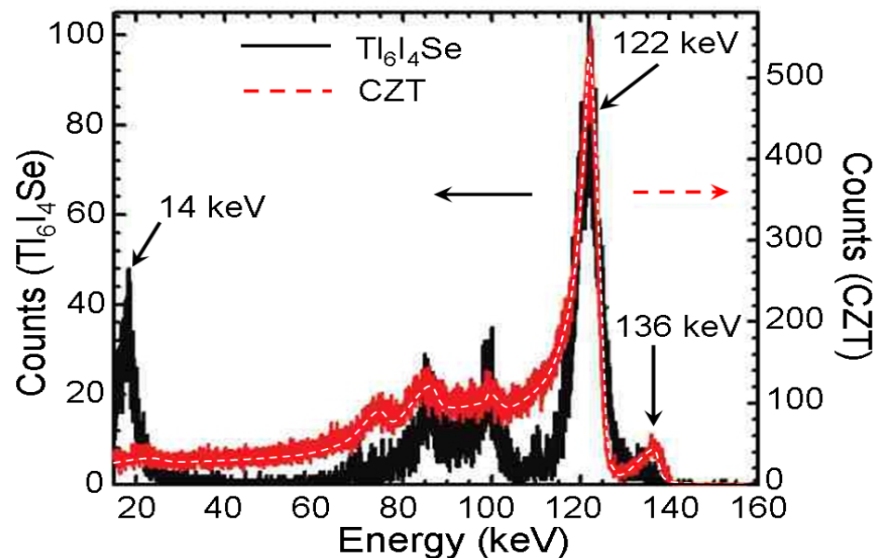
HgI₂ 5 mm², 200 μm thick detector at 0°C. ΔE at 5.9 keV = 198 eV (Iwanczyk *et al.* 1989)



GaAs 0.5 x 0.5 x 0.2mm³ detector at -20°C. ΔE at 5.9 keV = 150 eV (courtesy S. Nennonen)

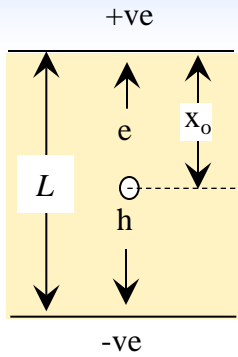


CdTe 1cm², 2.1 mm thick detector cooled to -35°C. ΔE at 662 keV was 3.5 keV (Khusainov *et al.* 1999).



Tl₆I₄Se, 6×4×2 mm³ detector. ΔE at 122 keV = 5.7 keV (Johnsen *et al.* 2011)

Charge transport described by the Hecht relation



$$CCE = \frac{Q}{Q_0} = \frac{\lambda_e}{L} \left[1 - \exp\left(-\frac{L-x_0}{\lambda_e}\right) \right] + \frac{\lambda_h}{L} \left[1 - \exp\left(-\frac{x_0}{\lambda_h}\right) \right]$$

λ_e	
1 m	Si
1 cm	CZT
1 mm	GaAs
1 μ m	GaP

$$\lambda_e = \mu_e \tau_e E \quad \lambda_h = \mu_h \tau_h E \quad \text{but } \mu\tau\text{'s rarely over } 10^{-4} \text{cm}^2 \text{V}^{-1} \text{ and } E \text{ usually } < 10^4 \text{ Vcm}^{-1}$$

For $\lambda/L < 1$ there will be a position dependence in the collected charge and spectral broadening

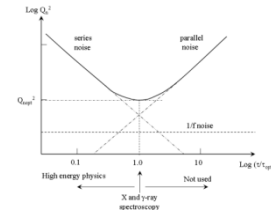
For the general case of $\lambda_e \neq \lambda_h$, the relative broadening is given by

$$\left(\frac{\sigma_c^2}{E} \right)^2 = \frac{2\lambda_e^2 \lambda_h^2}{L^3 (\lambda_e - \lambda_h)} \left(e^{-L/\lambda_e} - e^{-L/\lambda_h} \right) - \frac{1}{L^4} \left[\lambda_e^2 \left(e^{-L/\lambda_e} - 1 \right) + \lambda_h^2 \left(e^{-L/\lambda_h} - 1 \right) \right]^2$$

$$- \frac{\lambda_e^3}{2L^3} \left(e^{-2L/\lambda_e} - 1 \right) - \frac{\lambda_h^3}{2L^3} \left(e^{-2L/\lambda_h} - 1 \right)$$

Bottom line - spectroscopy dominated by the carrier with the poorest transport properties

Three main noise components comprise the resolution function ΔE



For RC-RC shaping

Fano noise $F = \frac{\sigma_{\text{exp}}^2}{\text{var}_{\text{poisson}}} \Rightarrow \sigma_F^2 = FE\varepsilon$

Electronic noise $\Delta e = \frac{2.355 \varepsilon \text{ ENC}}{e}$

$$\text{ENC}^2 = \left(\frac{\varepsilon^2}{8}\right) \left[\left(2eI + \frac{4kT}{R_b}\right) \tau + \left(4kTR_s + v_{na}^2\right) C_d^2 \frac{1}{\tau} + 4A_f C_d^2 \right]$$

↑
↑
↑

current noise (parallel)
voltage noise (series)
1/f noise

Charge trapping noise

$$\left(\frac{\sigma_c^2}{E}\right)^2 = \frac{2\lambda_e^2 \lambda_h^2}{L^3(\lambda_e - \lambda_h)} \left(e^{-L/\lambda_e} - e^{-L/\lambda_h}\right) - \frac{1}{L^4} \left[\lambda_e^2 \left(e^{-L/\lambda_e} - 1\right) + \lambda_h^2 \left(e^{-L/\lambda_h} - 1\right)\right]^2 - \frac{\lambda_e^3}{2L^3} \left(e^{-2L/\lambda_e} - 1\right) + \frac{\lambda_h^3}{2L^3} \left(e^{-2L/\lambda_h} - 1\right)$$

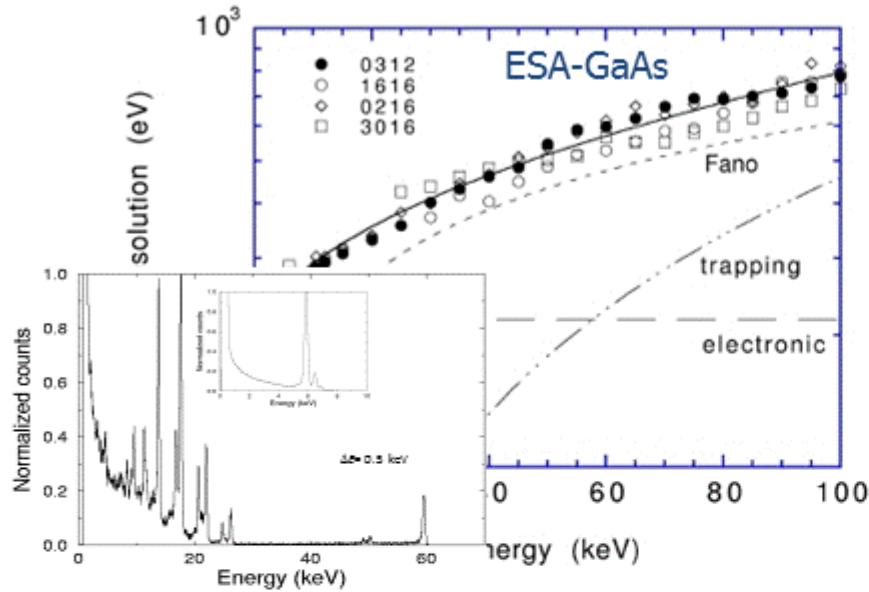
$$\Delta E = f(\sigma_F^2, \sigma_e^2, \sigma_c^2)$$

$$\Delta E = 2.355 \sqrt{F \varepsilon E_0 + (\Delta e / 2.355) + a_1 E_0^{a_2}}$$

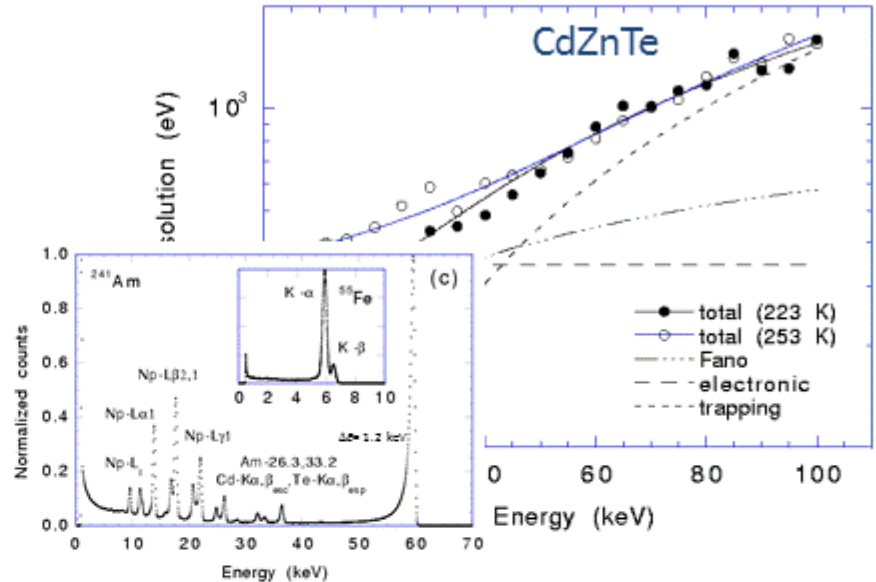
assuming all components are normally distributed

Effect of $\mu\tau$ on performance – smaller the $\mu\tau$ the poorer the performance or thinner the detector

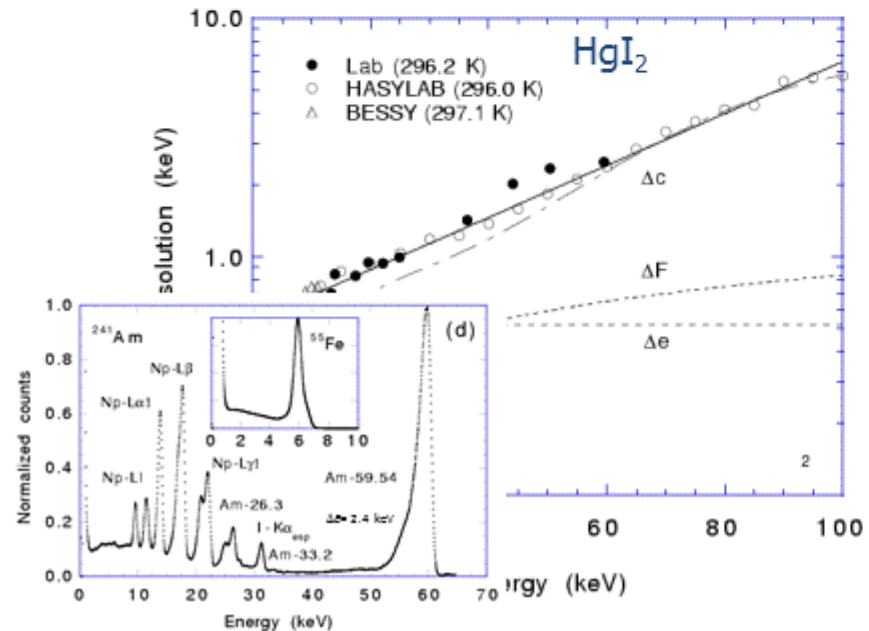
$\mu\tau \sim 10^{-2} \Rightarrow$ Fano limited



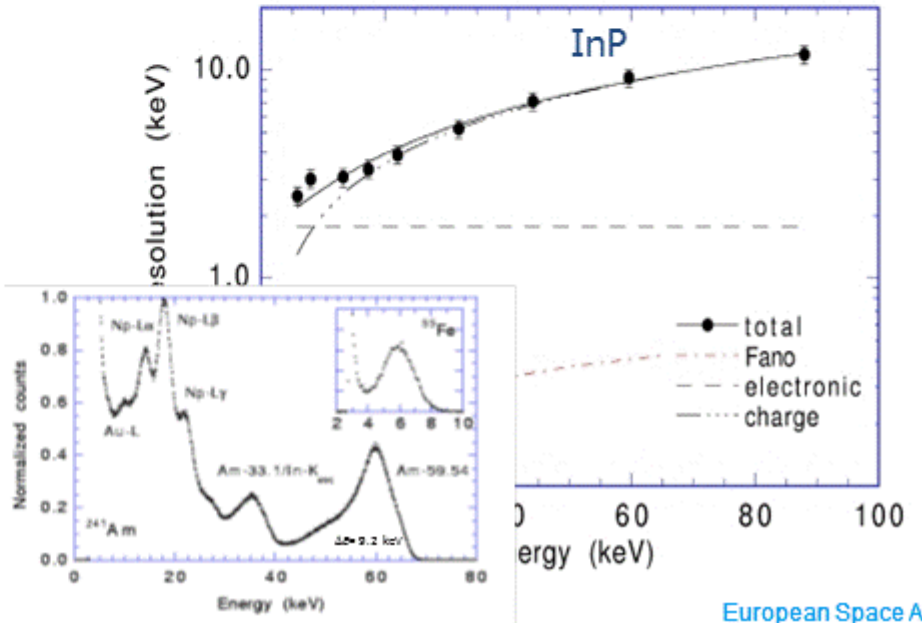
$\mu\tau \sim 10^{-3} \Rightarrow$ partially Fano limited



$\mu\tau \sim 10^{-4} \Rightarrow$ not Fano limited



$\mu\tau \sim 10^{-5} \Rightarrow$ what's Fano limited ?



- 1) Poor transport parameters
- 2) Crystal purity/stoichiometry
- 3) Thermal effects
- 4) Polarization
- 5) Radiation effects

Group III-V Materials

Group II-VI Materials

Physical Properties – Group III-V Materials

Physical Properties – Group II-VI Materials

Material	Crystal Structure	Pearson symbols/Space /Point group	Lattice constants <i>a</i> or <i>a</i> , <i>c</i> (nm)	Atomic numbers	Av. Mol. weight	Density (g cm ⁻³)	Melting point (K)	Icnicity <i>f_i</i>	KH (kg mm ⁻²)
InSb	ZB	cF8, F43m(T _d ²)	0.648	49, 51	236.6	4.78	797	0.321	220
InAs	ZB	cF8, F43m(T _d ²)	0.606	49, 33	189.7	4.68	1210	0.357	430
InP	ZB	cF8, F43m(T _d ²)	0.587	49, 15	145.8	4.79	1335	0.421	460
InN	W	hP4, P6 ₃ mc(C _{6v} ⁴)	0.354, 0.870	49, 7	128.8	6.81	2146	0.578	1140
GaSb	ZB	cF8, F43m(T _d ²)	0.610	31, 51	191.5	5.61	991	0.261	450
GaAs	ZB	cF8, F43m(T _d ²)	0.564	31, 33	144.6	5.32	1513	0.310	750
GaP	ZB	cF8, F43m(T _d ²)	0.545	31, 15	100.7	4.14	1730	0.327	964
β-GaN	ZB	cF8, F43m(T _d ²)	0.451	31, 7	83.7	6.15	3246 ²	0.500	1830
α-GaN	W	hP4, P6 ₃ mc(C _{6v} ⁴)	0.319, 0.518	31, 7	83.7	6.07	2791	0.500	1200-1700
BAAs	ZB	cF8, F43m(T _d ²)	0.478	5, 33	85.7	5.22	2027	0.044	1937
BP	ZB	cF8, F43m(T _d ²)	0.4538	5, 15	41.8	2.97	3300	0.032	3263
β-BN	ZB	cF8, F43m(T _d ²)	0.362	5, 7	24.8	3.48	3246	0.256	6730-7648
α-BN	H	hP4, P6 ₃ /mmc(D _{6h})	0.250, 0.666	5, 7	24.8	3.28	2873 ²	0.221	1489
AlSb	ZB	cF8, F43m(T _d ²)	0.614	13, 51	148.7	4.22	1338	0.250	408
AlAs	ZB	cF8, F43m(T _d ²)	0.566	13, 33	101.9	3.76	1710	0.274	510
AIP	ZB	cF8, F43m(T _d ²)	0.546	13, 15	58.0	2.36	2823	0.307	561
AlN	W	hP4, P6 ₃ mc(C _{6v} ⁴)	0.311, 0.498	13, 7	41.0	3.26	3487	0.449	1020-1427

¹(H) = parallel to c axis, (L) perpendicular to c axis
²sublimes/decomposes

Material	Crystal Structure	Pearson symbols/Space /Point group	Lattice Constants <i>a</i> or <i>a</i> , <i>c</i> (nm)	Atomic Numbers	Av. Mol. Weight	Density (g cm ⁻³)	Melting point (K)	Icnicity <i>f_i</i>	KH (kg mm ⁻²)
HgTe	ZB	cF8, F43m(T _d ²)	0.646	80, 52	328.2	8.12	943	0.650	23.5-37.7
HgSe	ZB	cF8, F43m(T _d ²)	0.609	80, 34	279.6	8.22	1270	0.680	23.5
α-HgS	W	hP6, P6 ₃ mc(C _{6v} ⁴)	0.415, 0.950	80, 16	232.7	8.19	1093	0.790	91
β-HgS	ZB	cF8, F43m(T _d ²)	0.585	80, 16	232.7	7.73	857	0.790	138 ^a
CdTe	ZB	cF8, F43m(T _d ²)	0.648	48, 52	240.0	5.85	1366	0.675	45.9-61.2
CdSe (c)	ZB	cF8, F43m(T _d ²)	0.607	48, 34	191.4	5.67	1512	0.699	130
CdSe	W	hP4, P6 ₃ mc(C _{6v} ⁴)	0.430, 0.701	48, 34	191.4	5.81	2023	0.699	91.8
CdS (c)	ZB	cF8, F43m(T _d ²)	0.582	48, 16	144.5	4.87	1748	0.685	125
CdS (h)	W	hP4, P6 ₃ mc(C _{6v} ⁴)	0.414, 0.671	48, 16	144.5	4.83	1748	0.685	123-235
ZnTe	ZB	cF8, F43m(T _d ²)	0.610	30, 52	193.0	6.34	1568	0.609	61.2-91.8
ZnSe (c)	ZB	cF8, F43m(T _d ²)	0.567	30, 34	144.3	5.26	1799	0.630	139.7-186.6
β-ZnS	ZB	cF8, F43m(T _d ²)	0.541	30, 16	97.5	4.08	1991 ^b	0.623	178
α-ZnS	W	hP4, P6 ₃ mc(C _{6v} ⁴)	0.382, 0.626	30, 16	97.5	4.08	2196	0.623	178
ZnO	ZB	cF8, F43m(T _d ²)	0.463	30, 8	81.4	5.68	2248	0.616	5.0 (M ^a)
ZnO	W	hP4, P6 ₃ mc(C _{6v} ⁴)	0.3250, 0.5204	30, 8	81.4	5.61	1975 ^b	0.616	407.9 ^a
β-MgTe	W	hP4, P6 ₃ mc(C _{6v} ⁴)	0.4530, 0.7406	25, 52	151.9	3.81	1360	0.554	143
β-MgSe	NaCl	cF8, Fm3m(O _h ²)	0.589	12, 34	103.3	4.20	1560	0.790	152
β-MgS	NaCl	cF8, Fm3m(O _h ²)	0.520	12, 16	56.4	2.86	2783	0.786	3.5 (M ^a) ^e

^aestimated
^bdecomposes/sublimes
^cMohs scale
^dhardest of the II-VI compounds
^evalue given for its mineral form, mningerite

Electronic Properties – Group III-V Materials

Electronic Properties – Group II-VI Materials

Material	Type	Bandgap <i>p</i> (eV)	Pair Energy (eV)	$\epsilon_r(0)^1$	Resistivity (Ω-cm)	Electron Mobility (cm ² V ⁻¹ s ⁻¹)	Hole Mobility (cm ² V ⁻¹ s ⁻¹)	$\mu_e\tau_e$ (cm ² V ⁻¹)	$\mu_h\tau_h$ (cm ² V ⁻¹)
InSb	D	0.18	1.2	17.7	~100 @ 4K	80000	1250	7×10 ⁻⁵	
InAs	D	0.354	2.0	15.1	0.03	33000	460		
InP	D	1.34	4.2	12.4	10 ⁸	4600	150	2×10 ⁻⁵	1×10 ⁻⁵
InN	D	1.89 ²		13.1(L), 14.4(H)		3200	<80		
GaSb	D	0.75		15.7	0.04	4000	700	1.4×10 ⁻⁵	
GaAs	D	1.425	4.35	13.1	10 ¹⁰	8500	400	1×10 ⁻⁴	4×10 ⁻⁶
GaP	I	2.27	6.5	11.1	10 ⁸ -10 ¹¹	110	75	1.4×10 ⁻⁶	
β-GaN	D	3.23		8.9	10 ⁶	760	250		
α-GaN	D	3.42		10.4(L), 9.5(H)	>10 ¹⁰	1500	30		
BAAs	I	1.85**		9.9					
BP	I	2.4	6.5	11.0	20	30-120	285-500		
BN (c)	I	6.4		7.1	10 ³	<200	<500		
BN (h)	I	5.2		7.04(L), 5.1(H)	10 ¹⁴				
AlSb	I	1.62	6.58	14.4	0.04-10 ⁷	200	420		
AlAs	I	2.15		10.9	0.2	200	100		
AIP	I	2.42		9.8	1×10 ⁻⁵	60	450		
AlN (h)	D	6.19		8.3(L), 8.9(H)	10 ¹³	300	14		

Material	Type	Bandgap (eV)	Pair Energy (eV)	Dielectric Constant $\epsilon_r(0)^3$	Resistivity (Ω-cm)	Electron Mobility (cm ² V ⁻¹ s ⁻¹)	Hole Mobility (cm ² V ⁻¹ s ⁻¹)	$\mu_e\tau_e$ (cm ² V ⁻¹)	$\mu_h\tau_h$ (cm ² V ⁻¹)
HgTe	SM	-0.14		20.8	10 ² -10 ³	25000	350		
HgSe	SM	-0.06		25.6		20000	2		
α-HgS	D	2.03		23.5(H), 18.2(L)	3450 (H), 11080 (L)	30(H), 10(L)			
β-HgS	SM	0.54		18.2		250			
CdTe	D	1.48	4.43	10.4	10 ⁸	1050	100	3.3×10 ⁻³	2×10 ⁻⁴
CdSe (c)	D	1.74	5.5	10.0	10 ⁷	800	50	7.2×10 ⁻⁴	7.5×10 ⁻⁵
CdSe (h)	D	1.75	5.5	9.3(L), 10.2(H)	10 ⁸	840	75	6×10 ⁻⁵	7.5×10 ⁻⁵
CdS (c)	D	2.42	6.3	5.4		340	50		
CdS (h)	D	2.51	7.8	8.3(L), 8.7(H)	10 ¹⁰	330	48	10 ⁻⁷	
ZnTe	D	2.28	7.0	10.4	10 ¹⁰	340	100	1.4×10 ⁻⁵	7×10 ⁻⁵
ZnSe (c)	D	2.63	8.0	9.2	2×10 ⁹	540	28	4×10 ⁻⁵	
β-ZnS (c)	D	3.58	8.2	8.9	10 ¹⁰	165	10		
α-ZnS (w)	D	3.91		8.6(L), 8.4(H)	10 ⁵ -10 ¹²	280(H), 165(L)	100-800		
ZnO (c)	D	3.35	7.5	9.0		200	180		
ZnO (w)	D	3.37		7.8(L), 8.8(H)	10 ⁸	250(H), 280(L)	125		
β-MgTe	D	3.49		6.1					
β-MgSe	D	4.05		5.2					
β-MgS	D	4.5 (77K)		4.5					

^a Early studies showed 1.9-2.05. A recent study claims a value of 0.7-0.8 [33] and is supported by measurement [34].

^{**} Calculated value [35]. Optical absorption measurements suggest a bandgap energy of 0.67 eV [36].

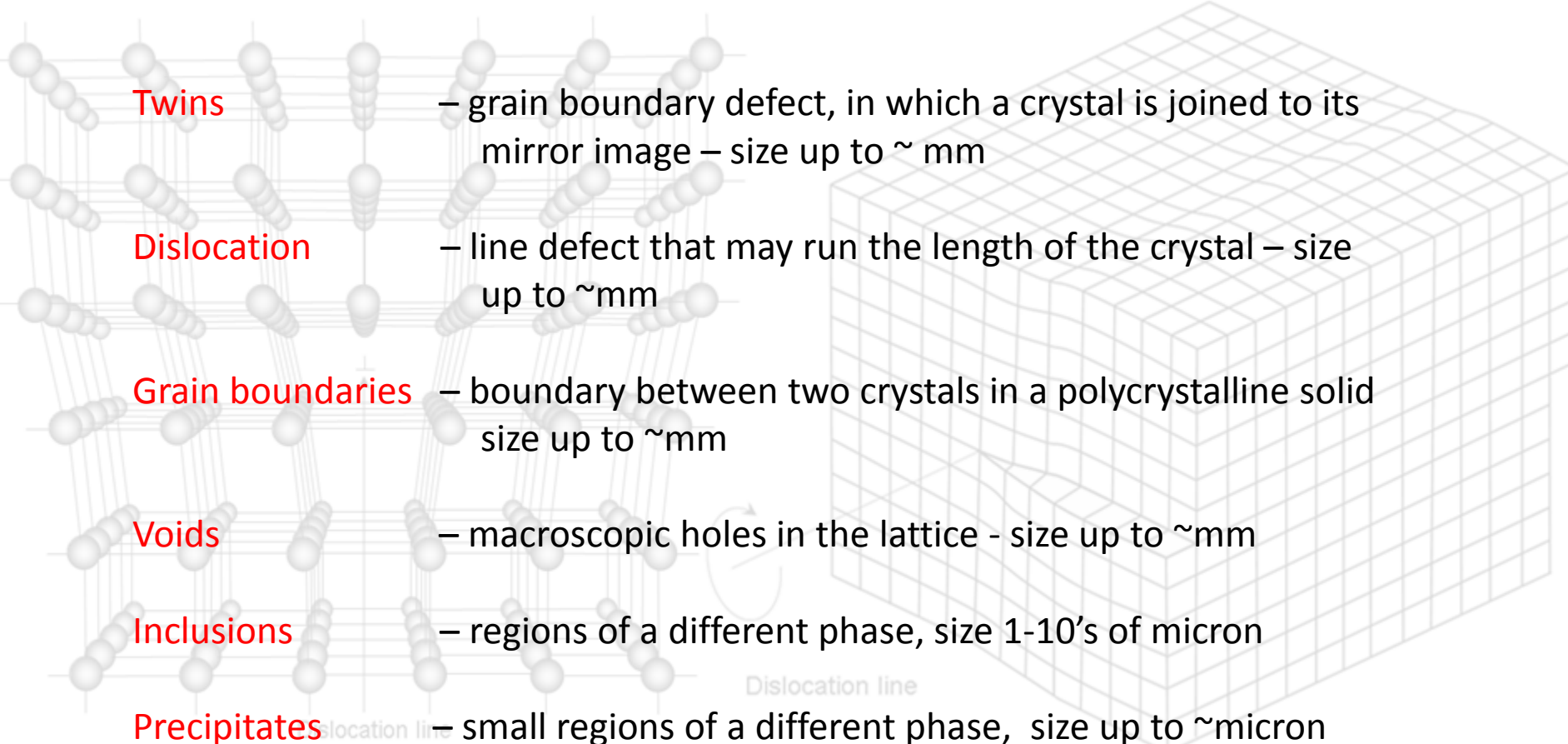
A. Owens, Compound Semiconductor Radiation Detectors, CRC Press (2012).

Room temperature properties of wide band gap compound semiconductor materials suitable for hard X- and γ -ray detectors. The abbreviations are: C = Czochralski, LEC = Liquid Encapsulated Czochralski, THM = Traveller Heater Method, BM = Bridgman Method, HPB = High Pressure Bridgman and VA=Vertical Ampoule Method.

Material	Growth method	Atomic Number	Density (g/cm ³)	Band gap (eV)	E _{pair} (eV)	Resistivity (Ω -cm)	$\mu\tau$ (e) Product (cm ² /V)	$\mu\tau$ (h) Product (cm ² /V)
Si	C	14	2.33	1.12	3.6	10 ⁴	4×10 ⁻¹	2×10 ⁻¹
Ge	C	32	5.33	1.57	4.6	50	1	1
GaAs	CVPE	31,33	5.32	1.43	4.2	10 ¹¹	10 ⁻²	5×10 ⁻⁴
InP	LEC	15.49	4.78	1.43	4.2	10 ⁶	5×10 ⁻⁶	< 2×10 ⁻⁵
CdTe	THM	48,52	6.2	1.44	4.4	10 ⁹	3×10 ⁻³	2.6×10 ⁻⁴
Cd _{0.9} Zn _{0.1} Te	HPB	48,30,52	5.78	1.57	4.6	10 ¹¹	7×10 ⁻³	9×10 ⁻⁵
PbI ₂	BM	82,53	6.2	2.3-2.6	4.9	10 ¹²	8×10 ⁻⁶	9×10 ⁻⁷
HgI ₂	VAM	80,53	6.4	2.13	4.2	10 ¹³	10 ⁻⁴	4×10 ⁻⁵
TlBr	BM	81,35	7.56	2.68	6.5	10 ¹²	3×10 ⁻⁵	1.5×10 ⁻⁶

For compounds, hole $\mu\tau$ is usually 10 times less than electron $\mu\tau$

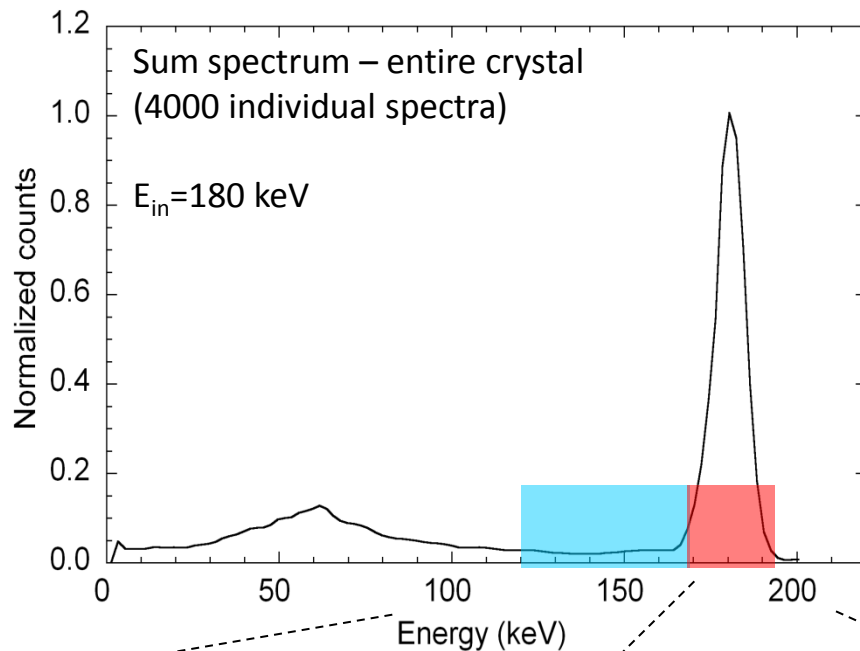
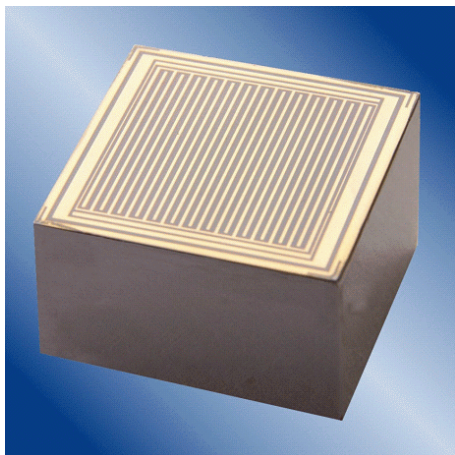
2) Crystal purity/stoichiometry - crystal defects



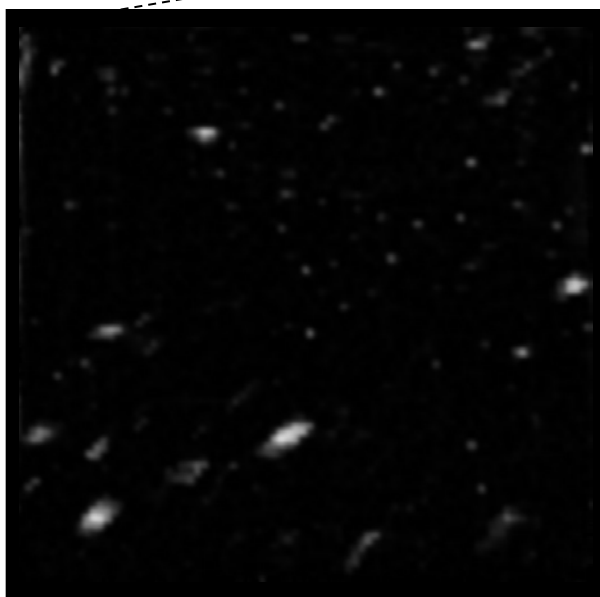
The diagram illustrates various crystal defects in a lattice structure. On the left, a 3D lattice of spheres is shown with several defects highlighted in red text. On the right, a larger 3D lattice structure is shown with a dislocation line indicated by a curved arrow and labeled 'Dislocation line'.

- Twins** – grain boundary defect, in which a crystal is joined to its mirror image – size up to \sim mm
- Dislocation** – line defect that may run the length of the crystal – size up to \sim mm
- Grain boundaries** – boundary between two crystals in a polycrystalline solid size up to \sim mm
- Voids** – macroscopic holes in the lattice - size up to \sim mm
- Inclusions** – regions of a different phase, size 1-10's of micron
- Precipitates** – small regions of a different phase, size up to \sim micron

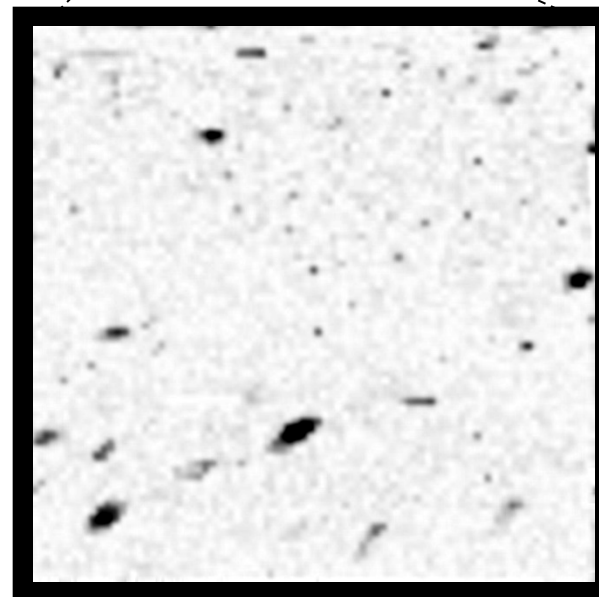
Effects of inclusions on spectra



ESRF
beamline ID15



Counts between 120-170 keV

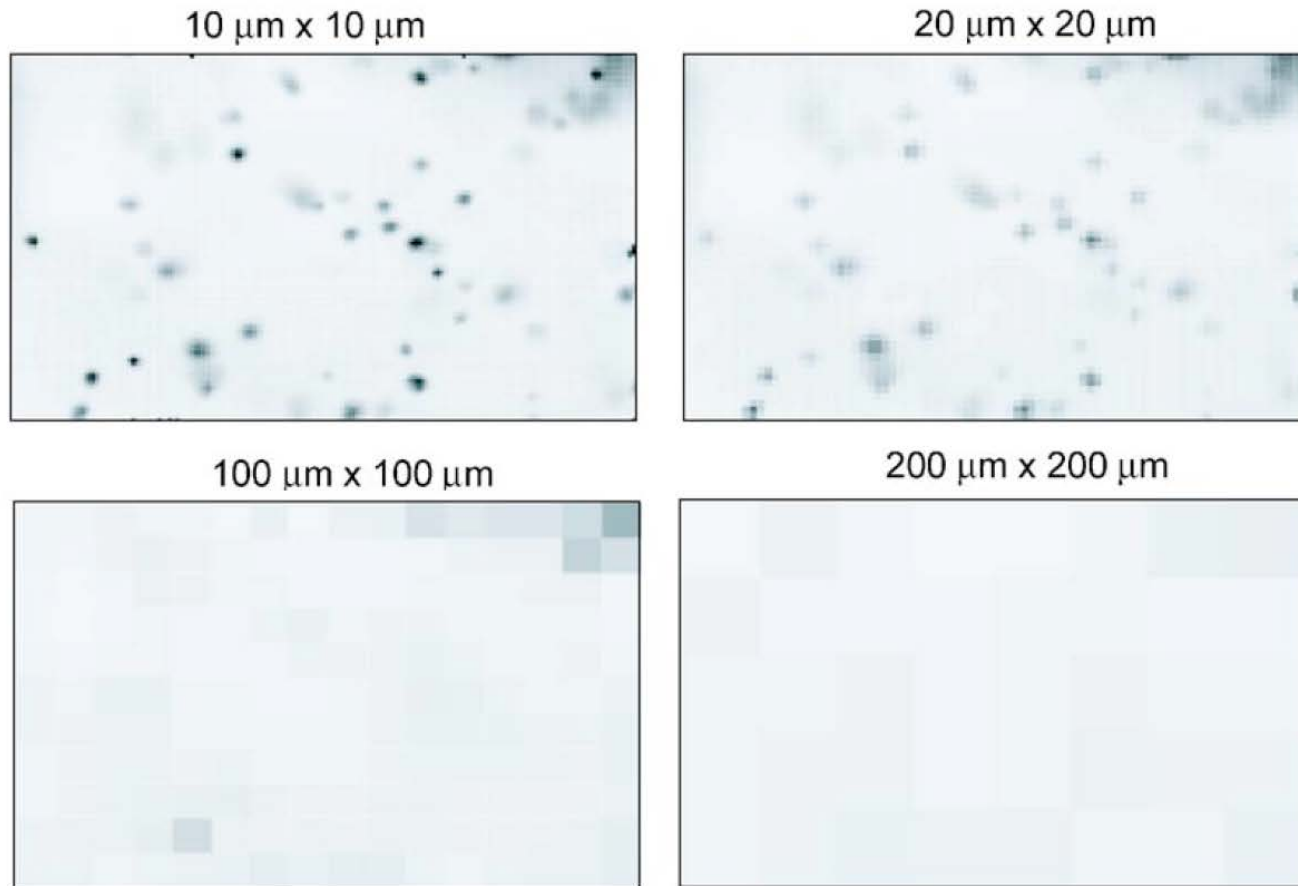


Counts between 170-193 keV

Coplanar grid CZT crystal imperfections

Why do some detectors have worse CCE and resolution than other similar detectors?

The X-ray world with finer spatial resolution

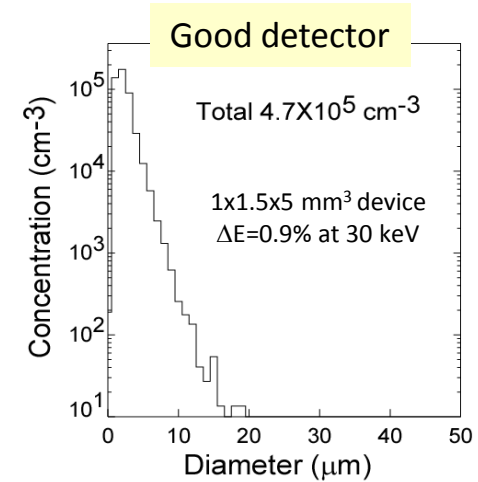
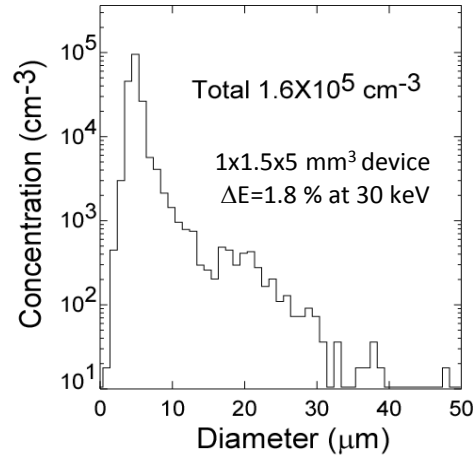
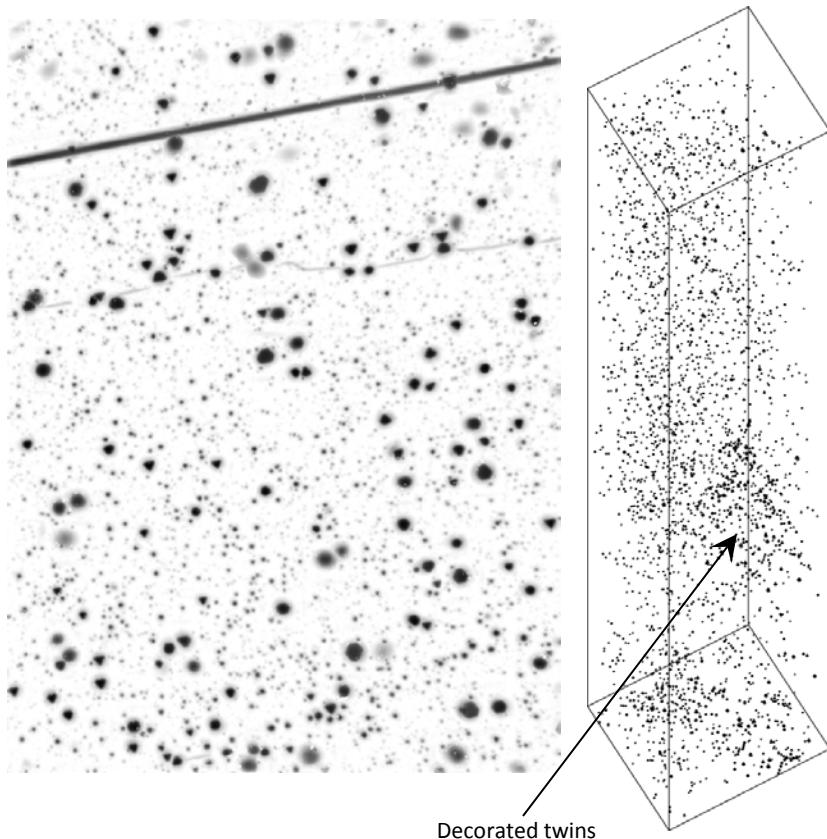


X-ray maps of the same areas of a 1mm thick CdZnTe device at different spatial resolutions

Carini et al., "Effect of Te precipitates on the performance of CdZnTe (CZT) detectors," Appl. Phys. Lett., **88** (2006) 143515-1

IR system allows “in-depth” images of Te inclusions, collapsed on a single plane from which it is possible to do a 3-D reconstruction of images. Can be used to measure sizes and inclusion concentration.

Example of the crystal with high concentration of Te inclusions. $1.1 \times 1.5 \times 10 \text{ mm}^3$



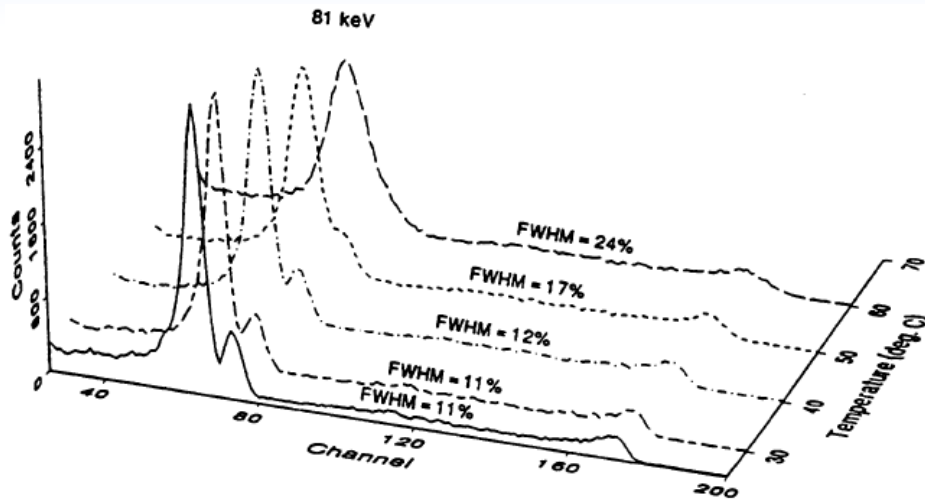
For each inclusion measure x,y,z, and diameter

Plug data into the model to generate X-ray response maps and pulse-height spectra

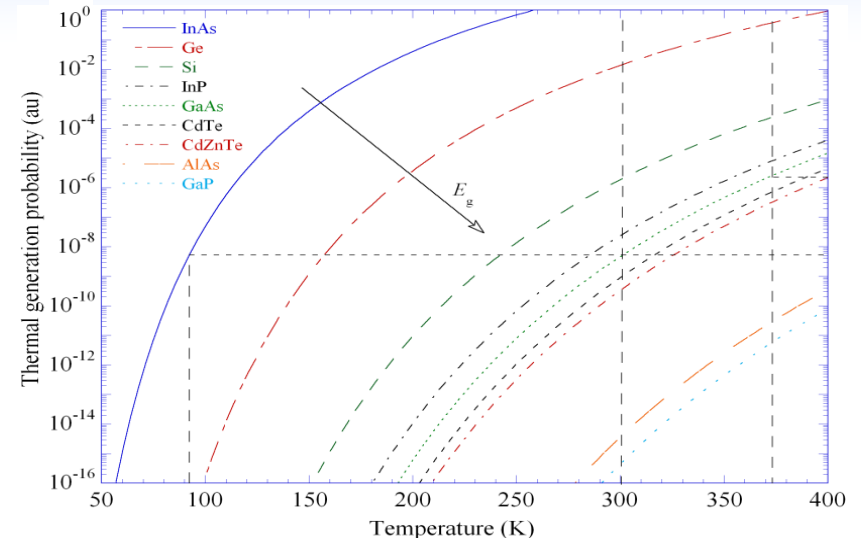
Currently, the model assumes that Te inclusions are opaque to carriers. It depends on a single adjustable parameter: the ratio between effective and actual size of inclusion

Performance limiting effects

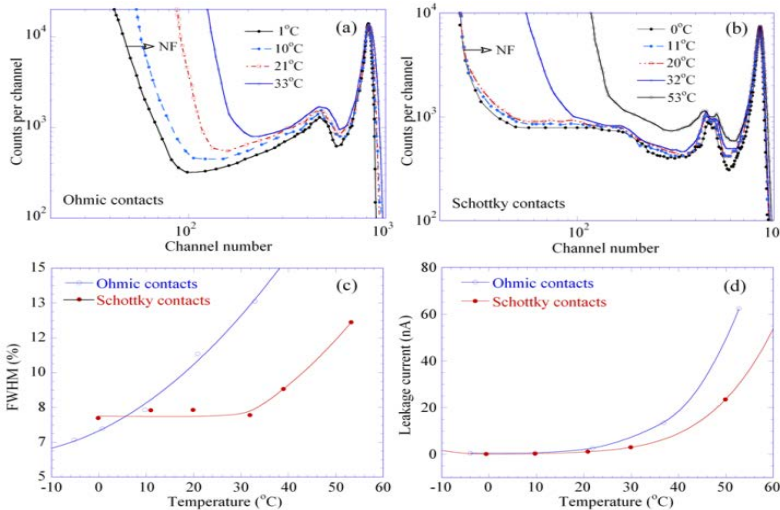
3) Temperature degradation effects



The progressive degradation of spectroscopic performance of a CdZnTe detector with increasing temperature (from Egareievwe, et al., *SPIE*, **2305** (1994) 167).



The probability of thermal electron-hole pair generation as a function of temperatures



Effects also depend on contacting system

Temperature dependencies

Intrinsic components $P(T) \sim T^{\frac{3}{2}} \exp\left(-\frac{E_g}{2kT}\right)$ $\mu_e \sim 8000 \left(\frac{300}{T}\right)^{2.3} \text{ cm}^2\text{V}^{-1}\text{s}^{-1}$ (GaAs)

External components – ohmic bulk leakage

$$I(T) \sim T^2 \exp\left(-\frac{E_{\text{eg}}(T)}{2kT}\right)$$

with blocking contact leakage

$$I(T) = A^* T^2 \exp\left(-\frac{e\phi_b}{kT}\right)$$

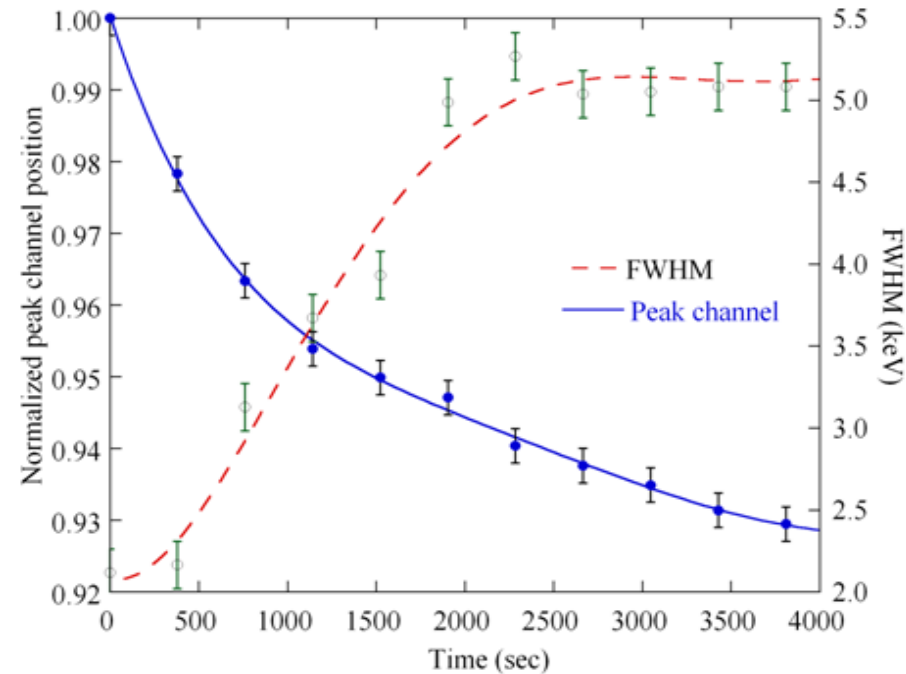
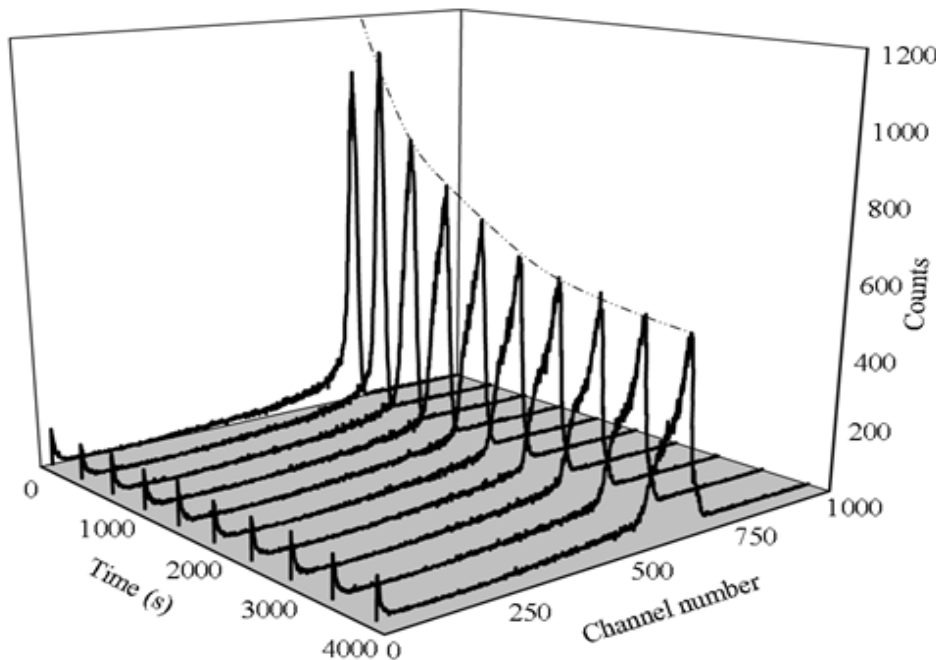
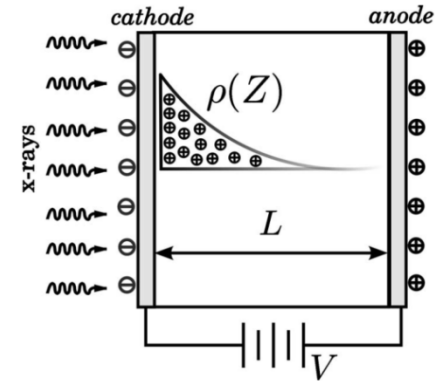
External components – surface leakage

$$I(T) = cT^2 \exp\left(-\frac{\phi_b}{kT}\right)$$

All strong dependencies

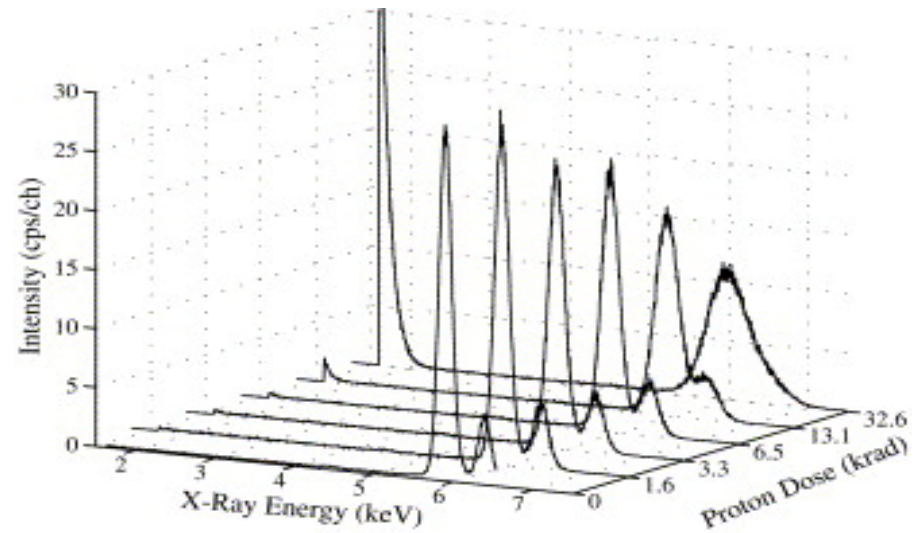
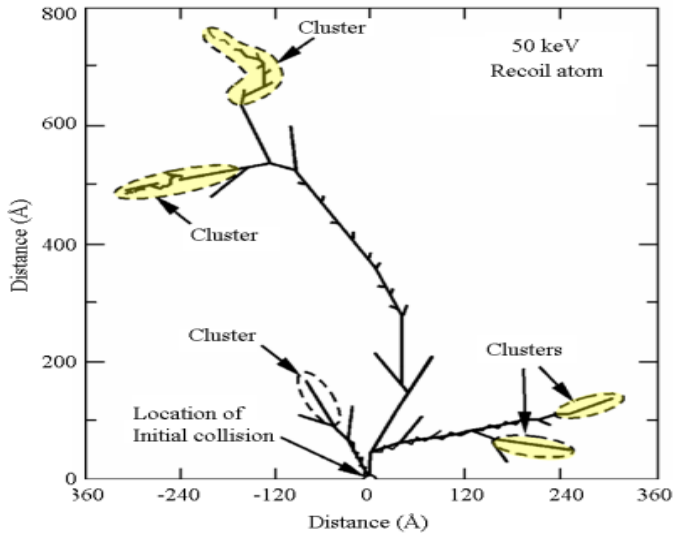
Time dependent build up of space charge due to mid-level traps (~ 0.8 eV) $\tau_{\text{ionization}} < \tau_{\text{deionization}}$

- bias induced
 - deep acceptor levels (depends on length of time bias applied, not on radiation level (examples, CdTe, HgI₂))
 - ionic conductivity (TlBr, AgCl)
- radiation induced - depends on radiation level and only relevant for high fluxes (examples include CdZnTe)



Polarization effects in a $5 \times 5 \times 2$ mm³ TlBr planar detector observed when exposed to a 50mm diameter 60 keV, 1 kHz, synchrotron beam

- a) **ionization**, in which charged particles ionize the atoms in a device causing an instantaneous release of charge. In bulk materials this charge dissipates by either diffusion or drift in an electric field. However, in structured devices the build-up of localized charge can damage devices - particularly in the vicinity of an interface.
- b) **displacement**, in which a device atoms are literally displaced and removed from their equilibrium positions introducing disorder into the crystal lattice structure. The consequences are the introduction of additional energy levels into the band gap which act as trapping and generation/ recombination centers, altering the semiconductors electronic properties.



Displacement damage in Si for the case where the energy transferred to the lattice site is more than 10^3 times greater than the displacement threshold energy. The displaced atom can initiate a “cascade”, displacing many thousands of atoms.

X-ray spectra for the irradiated and non-annealed Si pin-detectors (shaping time 6 μ s), after each proton exposure. A severe degradation in the energy resolution is already observed for proton doses of the order of 5–10 krad_(Si).

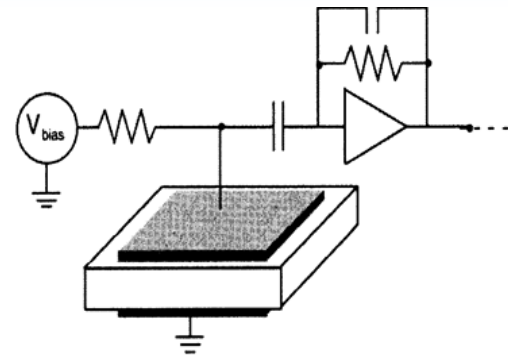
The factors affecting the calculated absorbed dose. For inter-comparison we list the absorbed doses for a proton irradiation of 2.66×10^9 p cm⁻². The data are ranked by the product of the average nuclear charge and atomic density. The last column gives the “Tolerance” index for each of the materials, which does not track the absorbed dose.

Compound	Bandgap eV	Atomic density cm ⁻³	Av. Nucl. Charge	Product cm ⁻³	Absorbed dose krad	Tolerance
CdZnTe	1.57	1.57×10^{22}	109.5	17.15×10^{23}	0.23	5
TlBr	2.68	1.60×10^{22}	53.2	8.52×10^{23}	0.60	3‡
Hgl ₂	2.13	0.84×10^{22}	92.1	7.81×10^{23}	1.05	1
GaAs	1.43	2.21×10^{22}	32.0	7.08×10^{23}	2.00	2
InP	1.35	1.98×10^{22}	27.1	5.38×10^{23}	1.31	4†
Si	1.12	4.97×10^{22}	5.29	2.63×10^{23}	2.00	6

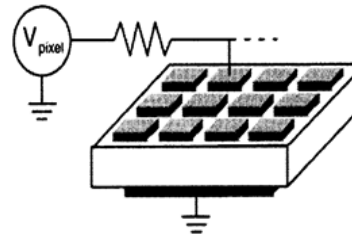
‡moved from 2nd position to 3rd because of much increased polarization effects.

†moved to 4th because of its very poor initial energy resolution and its electronic and structural similarity to GaAs.

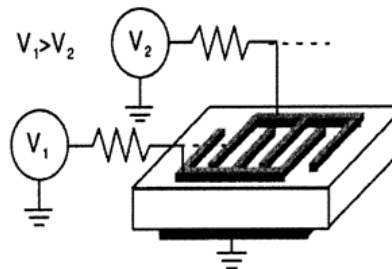
- Risetime discrimination
- Hemispherical geometries
- Frisch grid/ ring
- Small pixel effect
- Drift strip
- Ring drift
- Coplanar grid



Single element planar structure
(simple, thickness limited, ΔE heavily dependent on transport properties.)

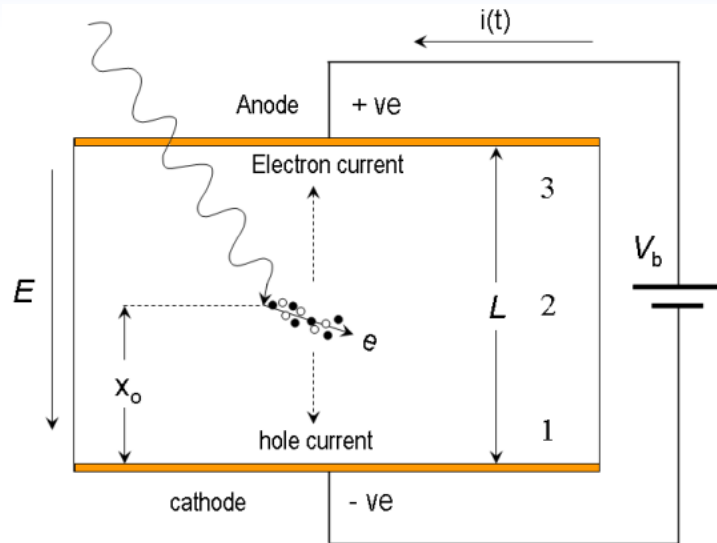


Pixel detector structure
Simple, small pixel effect – very good energy resolution, charge sharing complicated electronics/readout.



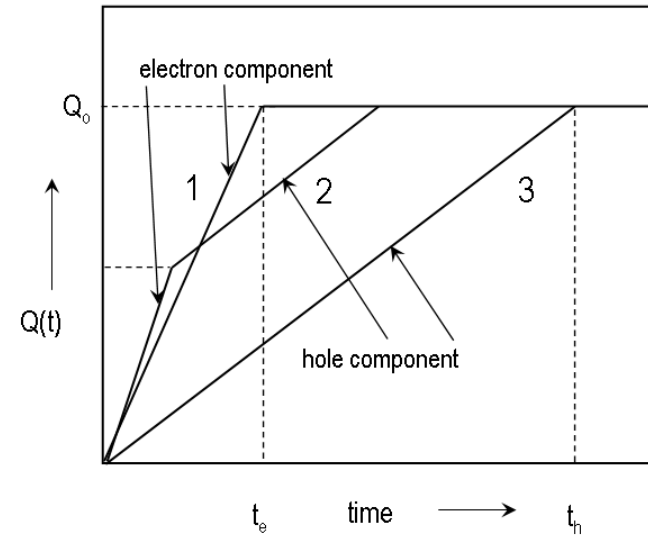
Co-planar grid structure
(good resolution, large volumes possible, complicated photolith.)

However, we need a difference of \sim a factor of 10 in the μ - τ products to be effective



$$t_e = \frac{L}{\mu_e E}$$

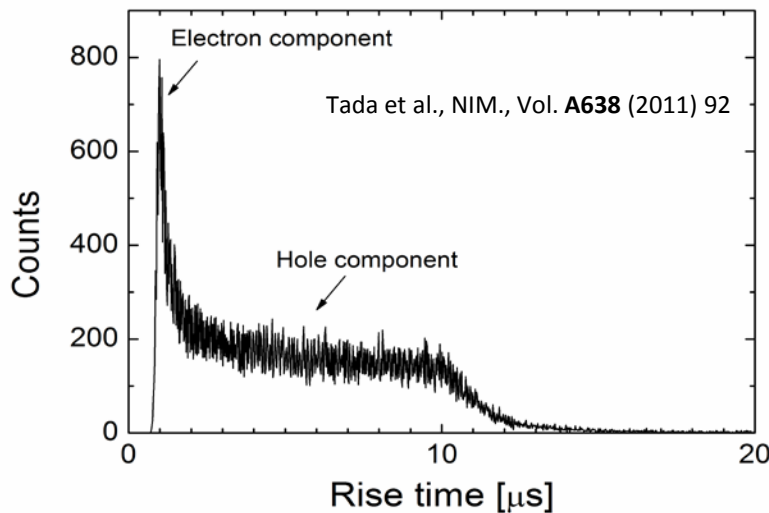
$$t_h = \frac{L}{\mu_h E}$$



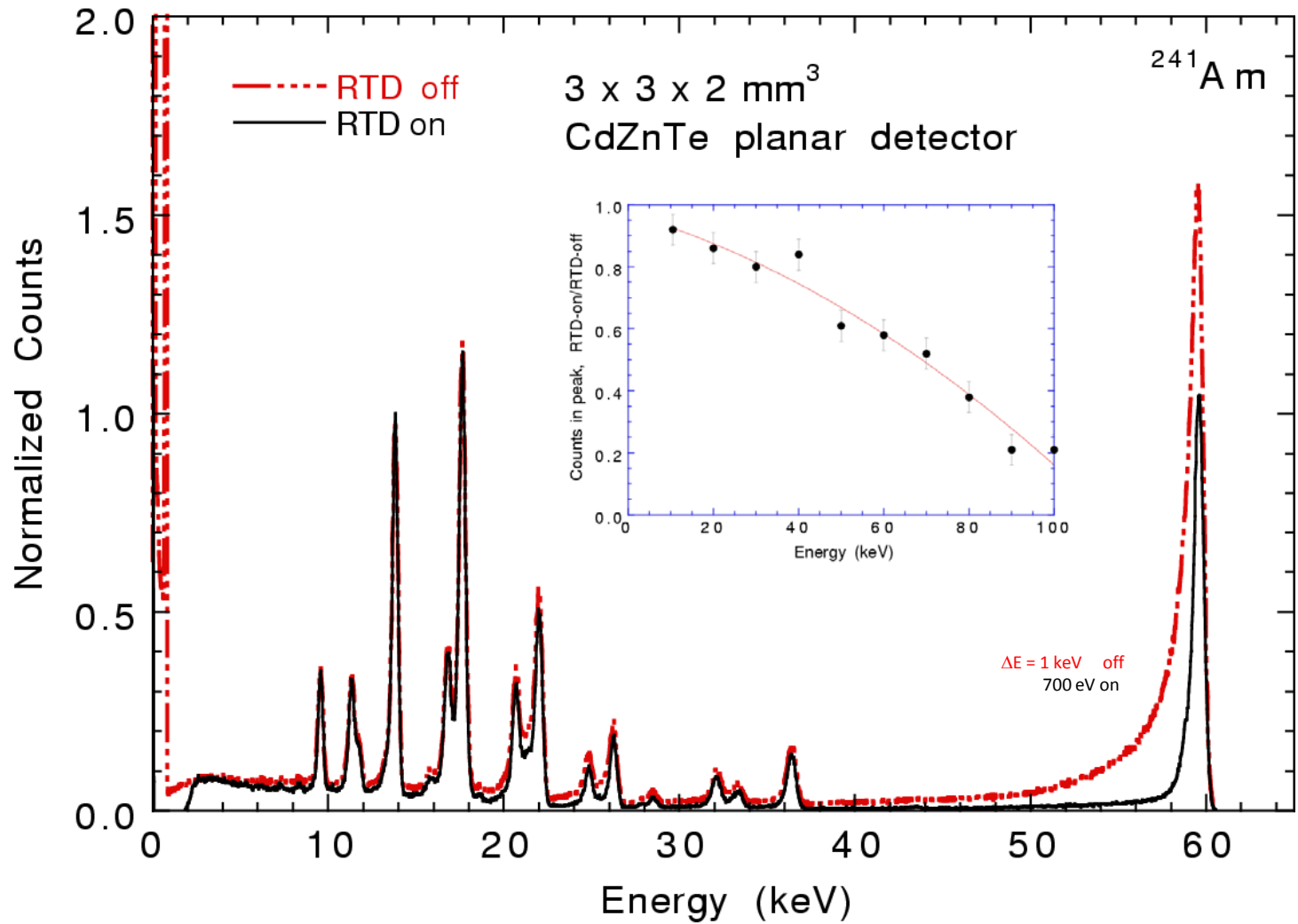
$$i = \frac{dQ}{dt} = q\vec{v} \cdot \vec{E}_w$$

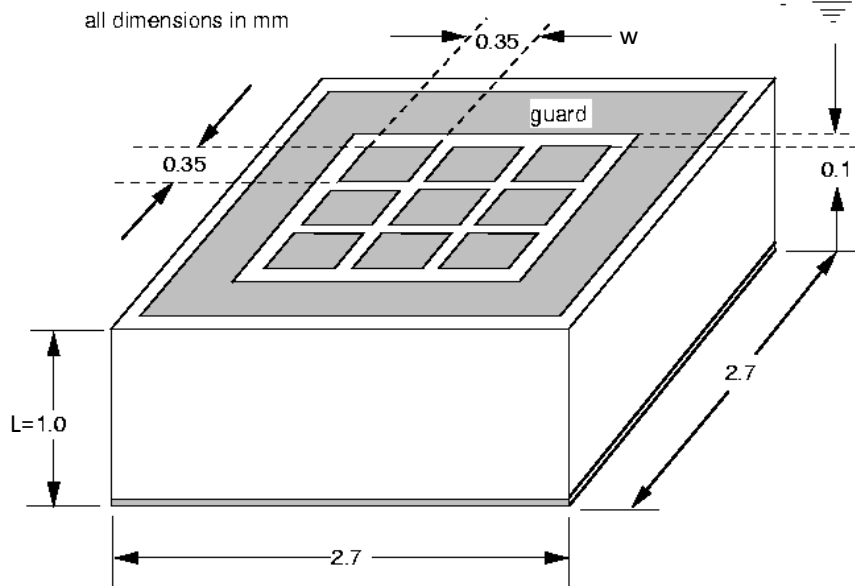
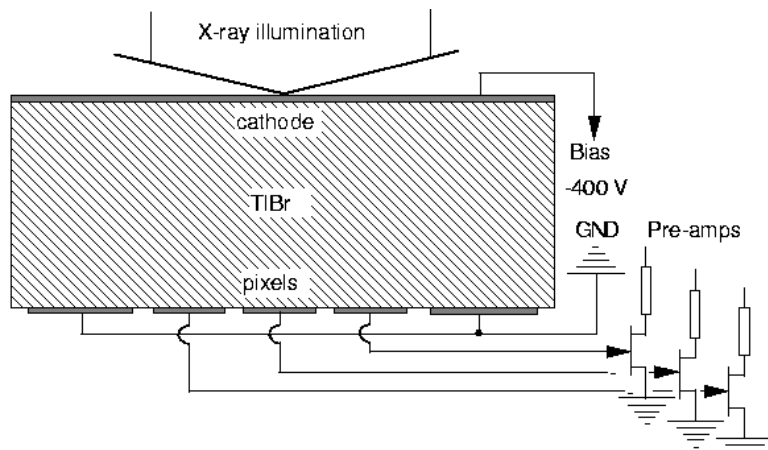
$$I_{eo} = Q_o \left(\frac{\mu_e E}{L} \right)$$

$$I_{ho} = Q_o \left(\frac{\mu_h E}{L} \right)$$

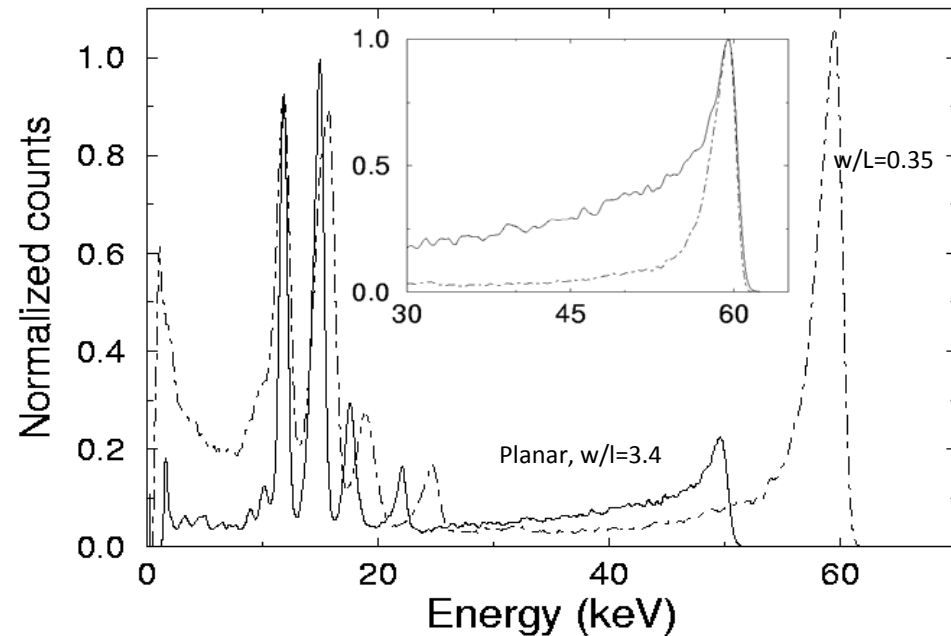
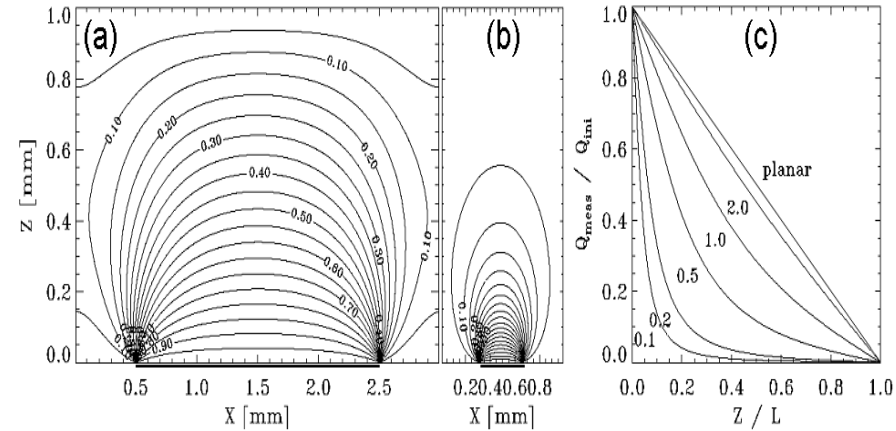


When $\mu_e \gg \mu_h$ the current pulse induced by the electrons will have a much larger amplitude and shorter duration than that induced by the holes. For interactions in the bulk of the detector, the induced signal will be a composite of electron and hole components whose relative strengths will now depend on the depth of the interaction. In RTD methods, all pulses whose risetime exceeds a pre-set threshold are rejected - in fact, those events that would normally lie in the tail.



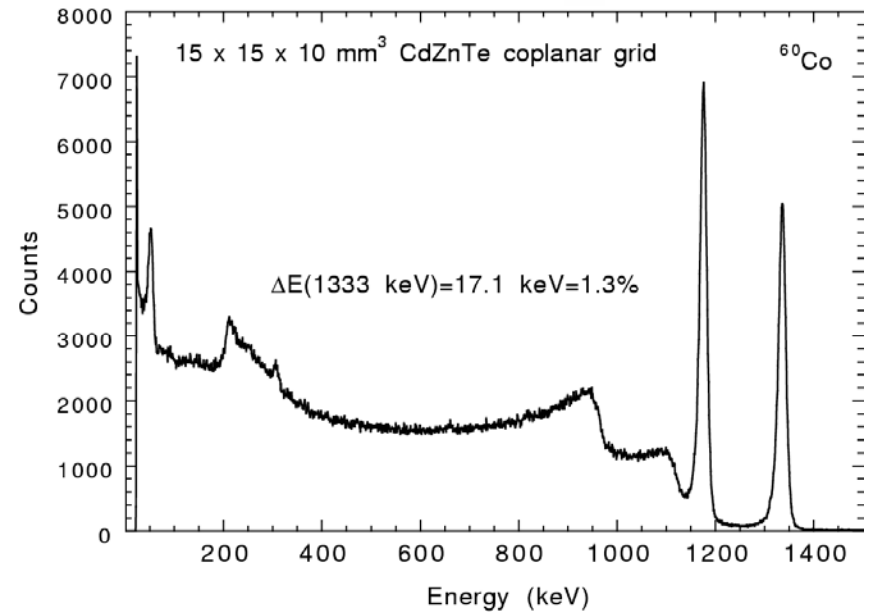
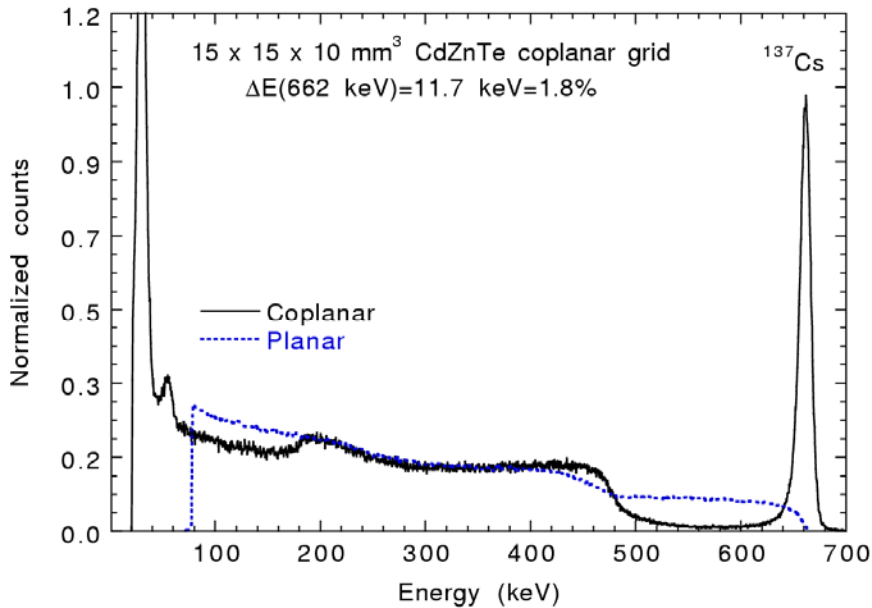
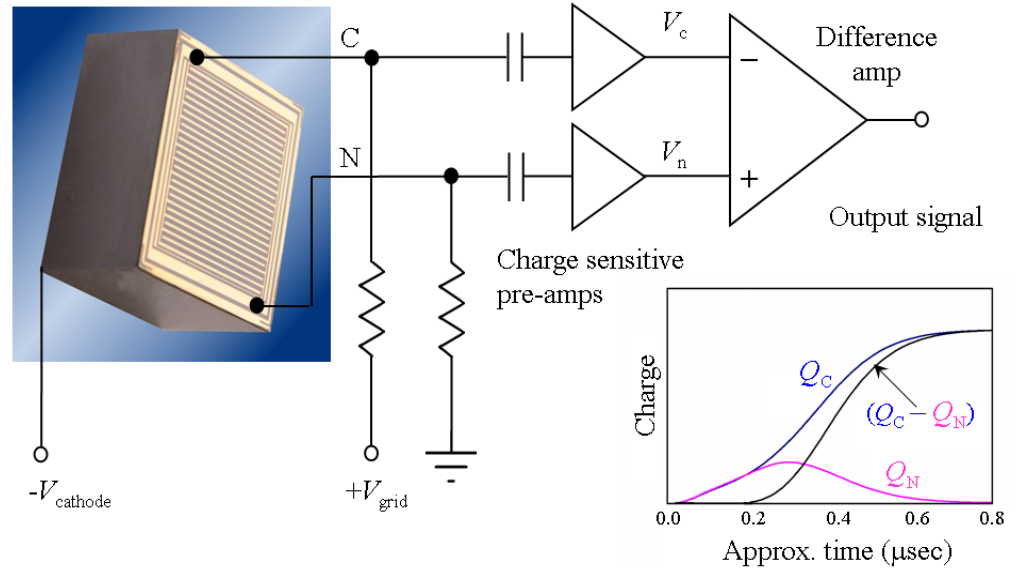
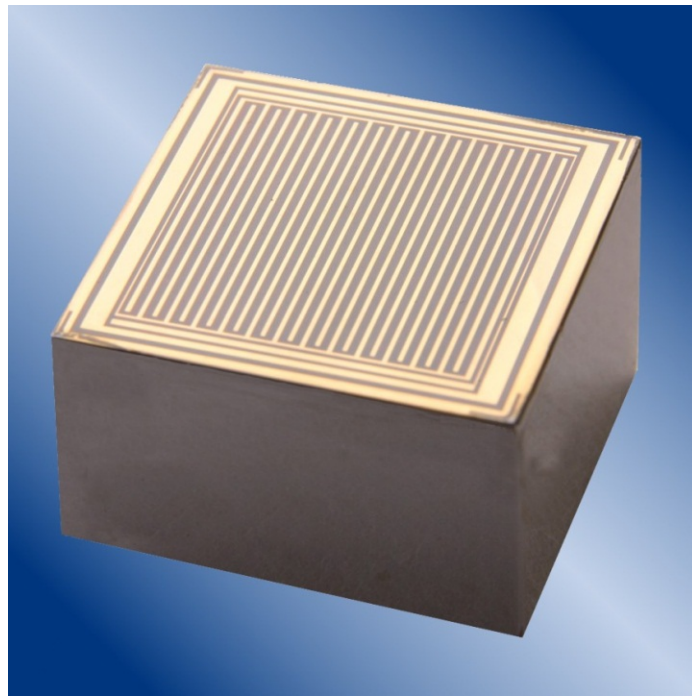


Weighting potential distributions



Coplanar grid technique

Luke, IEEE Trans. Nuc. Sci., Vol. **NS-42** (1995) pp. 207–213



The wish list – towards the ideal detector

conventional

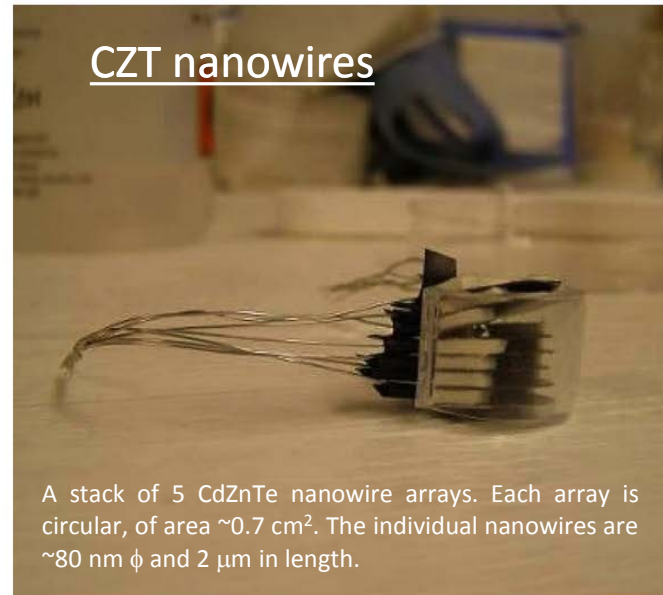
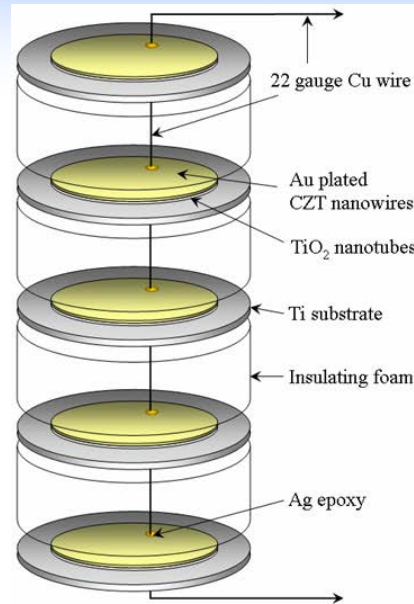
Summary of desirable material parameters for the development of the next generation of semiconductor detectors, in the form of a list of the minimum material and/or preferred values. Because of the uncertainty in end applications and compatibility between requirements, some of the recommendations are by necessity subjective.

Parameter	Minimum or recommended value	Reason/Comments
Composition	Binary (or pseudo binary)	To minimize stoichiometry errors.
Structure	Cubic (close packed)	To optimize density.
Density	$> 5 \text{ g cm}^{-3}$	To ensure good stopping power.
Growth technique	Epitaxial, FZ	Allows the possibility of integrated electronic structures.
Contact barrier height	$< 0.4 \text{ eV}$	To ensure the contacts "look" Ohmic (i.e., with a resistivity $< 10^{-3} \Omega \text{m}^2$).
Effective atomic number, Z_{eff}	> 40	For high stopping power.
Resistivity	$> 10^9 \Omega \text{ cm}$	To allow high biases to be applied.
Hardness	$> 500 \text{ kgf mm}^{-2}$ (Knoop scale)	Chosen to be high enough to allow the use of a range of mechanical processing and bonding technologies.
Bandgap	Indirect	To limit radiative recombination.
Bandgap energy	$1.4 < \epsilon_g < 2.2 \text{ eV}$	Lower limit for room temperature operation. Upper limit imposed by mobility losses due to polar lattice scattering.
Static dielectric constant, $\epsilon(0)$	< 5	To ensure low capacitance.
Ionicity	< 0.3 (Phillips scale)	Ionicity should be low to prevent problems with ionic conductivity and polarization
Majority carrier trapping centre density	$< 5 \times 10^{12} \text{ cm}^{-3}$	To ensure good charge collection.
Impurity concentration	$< 10^{15} \text{ cm}^{-3}$	Can adversely affect resistivity, mobilities and effective mass.
Mobility electrons	$> 500 \text{ cm}^2 \text{V}^{-1} \text{s}^{-1}$	Charge induction considerations
Mobility holes	10 or $500 \text{ cm}^2 \text{V}^{-1} \text{s}^{-1}$	Lower value if single carrier sensing is used, upper value if not.
Majority carrier lifetime	$> 20 \mu\text{s}$	To ensure reasonably high $\mu\text{-tau}$ products
Electron mobility-lifetime ($\mu\tau_e$)	$10^{-3} \text{ cm}^2 \text{V}^{-1}$	Minimum value really depends on application, X-rays or γ -rays.
Hole mobility-lifetime ($\mu\tau_h$)	$< 10^{-4}$ or $10^{-3} \text{ cm}^2 \text{V}^{-1}$	$(\mu\tau_h)$ should be $< 0.1 (\mu\tau_e)$ if single carrier sensing is employed.
Majority carrier effective mass	$0.1 m_0$	To ensure high speed operation.

- Engineered materials – lattice hybridization
- Reduced dimensionality materials
 - Quantum heterostructures
 - Radiation detection with nanosemiconductors (1-D)
 - Radiation detection based on 2-D materials
- Other degrees of freedom
 - Radiation detection based on Spintronics
 - Radiation detection based on Valleytronics
- Biological detection systems and intelligent photonics

Advantages

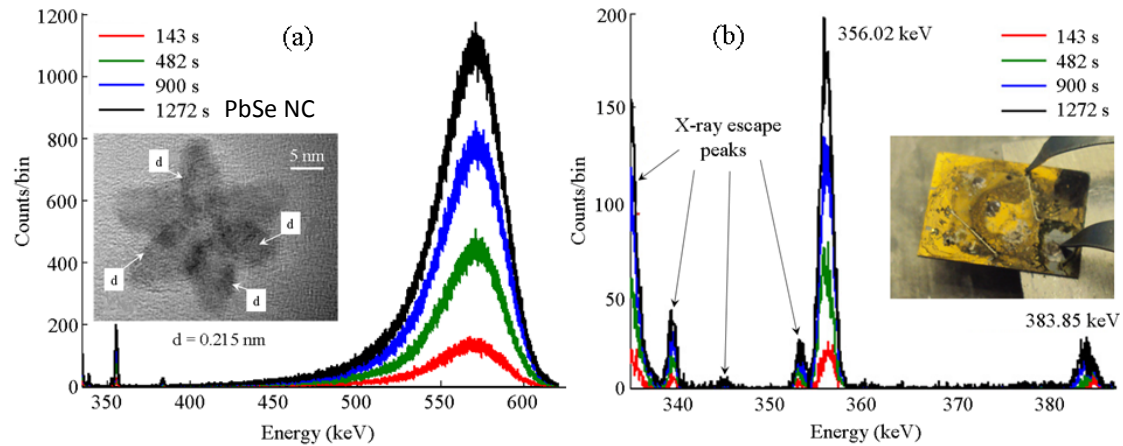
- Easy to manufacture
- Fabricate large detectors
- Can be grown by electrodeposition
- Better xtal perfection
- 1D conductors
- Biases can be low



PbSe nanocrystals



Detector $7 \text{ mm} \phi \times 5 \text{ mm}$ deep



ΔE at 662 keV same as HPGe

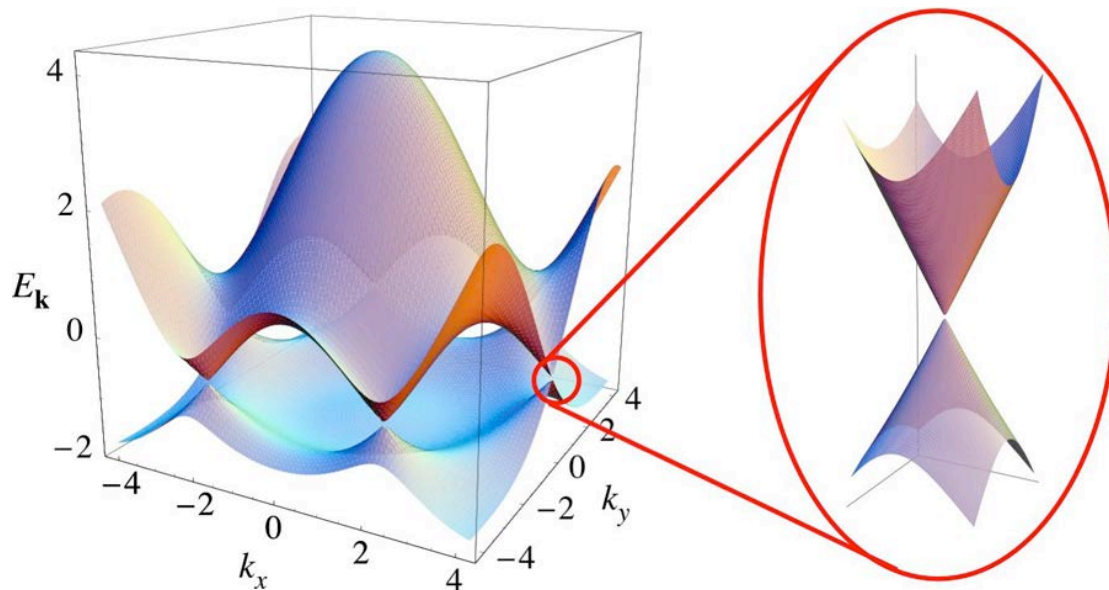
Energy-loss spectra measured from a ^{133}Ba and ^{241}Am source. The composite α -particle and γ -ray response is shown in (a) for a $1 \times 1 \text{ cm}$ thin (10's of μm) assembly of a conductive polymer and star-shaped PbSe nanoparticles. (b) An expansion of the ^{133}Ba γ -ray spectrum, in which the Pb and Se X-ray escape peaks are also apparent.

For a 3D periodic crystal structure, the energy bands appear parabolic in E, \mathbf{k} space near the conduction band minimum and valance band maximum and can be approximated by the well-known dispersion relationship

$$E(\mathbf{k}) = E_0 + \frac{\hbar^2(\mathbf{k})^2}{2m}$$

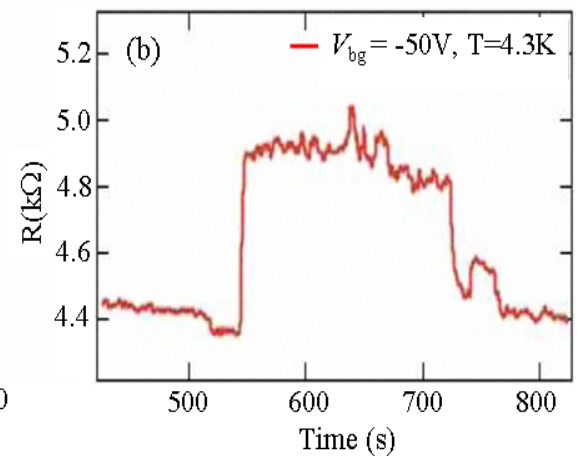
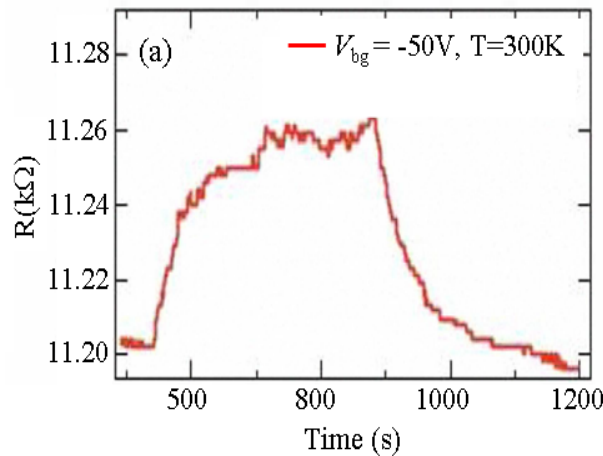
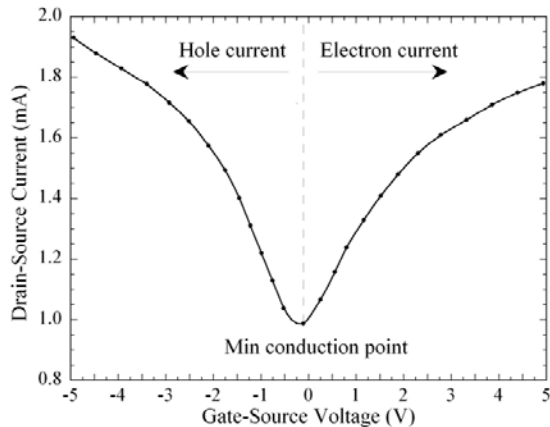
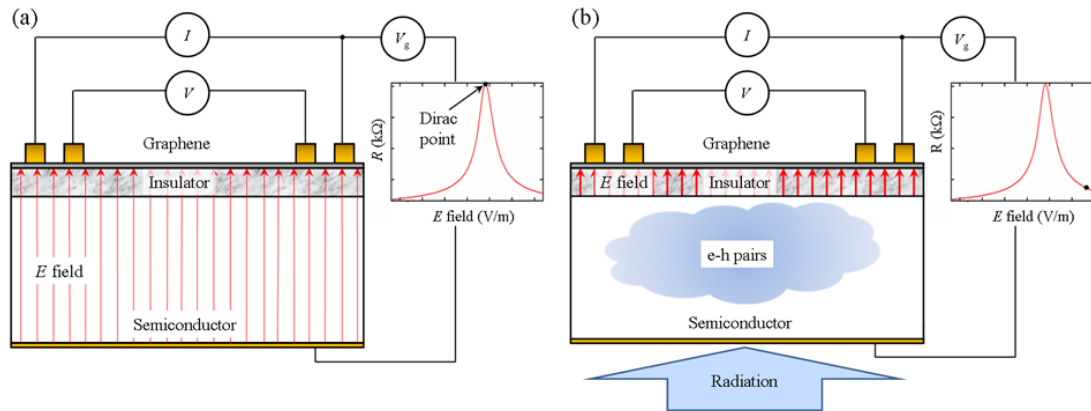
Here we see that the allowed energies of the carriers are dependent on their effective masses. However, in the 2D structure of graphene, the energy bands near the conduction band minima and valence band maxima are conical and actually touch at six points in \mathbf{k} space and the effective mass tends to zero – the so called K points. At these points, the dispersion relationship is given by

$$E(\mathbf{k}) = \pm \hbar v_F \sqrt{k_x^2 + k_y^2}$$



Which has no mass term. What this means is that while in standard semiconductors, the charge carriers can be described as electron waves obeying the Schrödinger effective-mass eqn., graphene electrons move according to the laws of relativistic quantum physics described by the mass-free Dirac eqn. Consequently, graphene has very high electron mobilities at room temperature, with values in excess of $15,000 \text{ cm}^2\text{V}^{-1}\text{s}^{-1}$.

A graphene FET (GFET) radiation detector - principle of operation. (a) A GFET consists of an absorber (undoped semiconductor), with an insulator buffer layer, which serves as a gate dielectric. V_g is the gate voltage applied to the sample. Current is supplied across the graphene sample, and the resistance of the graphene layer determined. In (b), incoming radiation produces ionization within the (intrinsic) semiconductor to create a conducting absorber. The gate voltage now only drops across the insulator. This results in an increased electric field, which is sensed by the graphene and its resistance changes as a result of the change in electric field as shown by the insets in the figure.



Left. GFET operation showing the variation of the drain-source current with gate source voltage using a thin p-type Si absorber. The curve reflects the Dirac curve and the device can be biased to collect either electrons or holes. (a) and (b). In (a) we show the response of a SiC based GFET to γ -rays and in (b), the response of a GaAs based GFET to X-rays. The initial rise in response corresponds to the point in time when a source is applied and the fall in response to when the radiation source is removed.

A. Patil et al., "Graphene Field Effect Transistor as Radiation Sensor", *IEEE Nucl. Sci. Symp. Conf. Rec.*, (2011) 455.

Tenent

Conventional detection systems only utilize the electrons charge

“The incremental advances in the current semiconductor nuclear detector technology will not be sufficient for developing the next generation of ultra sensitive, cost-effective detectors”

“Such developments will require the utilization of entirely new and transformative approaches”

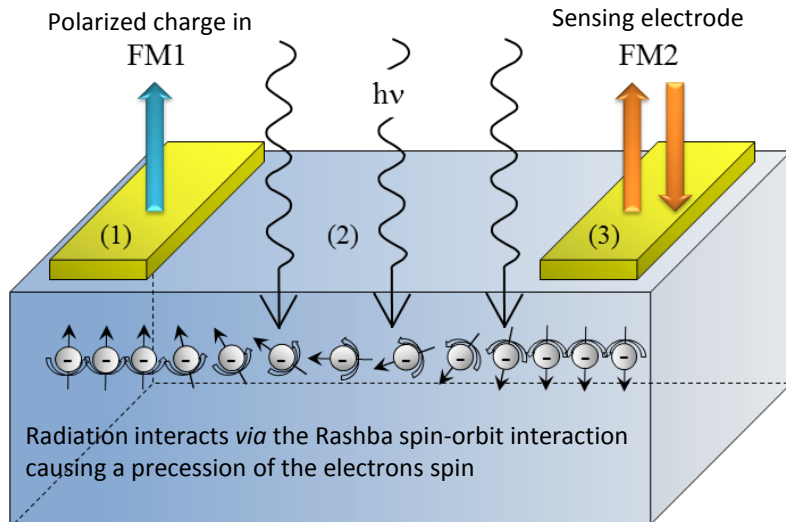
Gary et al., IEEE Trans Nucl. Sci. conf. record, Vol. (2012) 4152-4155.

Conventional detection systems only utilize the electrons charge

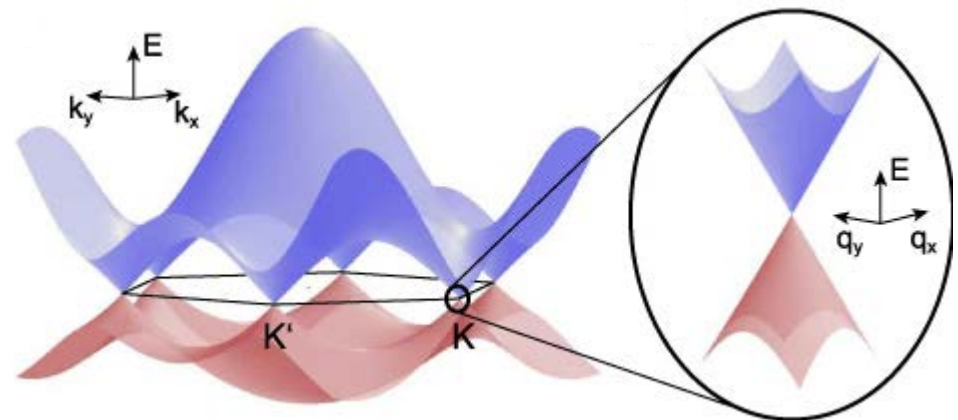
Use the more obscure internal degrees of freedom of the electron, for nonvolatile information processing

Spintronics¹

The idea is to fabricate device that operates using not just an electron's charge, but also its spin and associated magnetic moment. In an electron, spin behaves like angular momentum, but is not related to any real rotational motion. As a result, the spin of an electron can be switched much more quickly than charge can be moved round. Charge can also be collected in the usual way by applying a potential across the device. Spin is injected from a polarized source (such as a ferromagnetic metal (e.g., Ni or Fe), FM1) into the active semiconductor region. The polarised electrons then interact with the incident radiation changing the spin of the electrons. The new polarization of the electron is then sensed at the other end of the semiconductor by a second ferromagnetic electrode (FM2)



FM is a ferromagnetic metal such as Ni or Fe



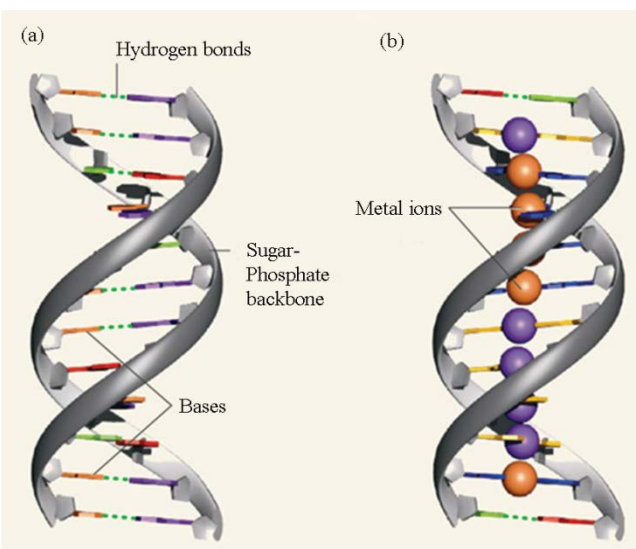
Valleytronics

Like spintronics, valley-based electronics, or valleytronics is another recent development that makes use of the more obscure internal degrees of freedom of the electron, for nonvolatile information processing. It relies on the fact that the conduction bands of some materials have two or more minima at equal energies but at different positions in momentum space. By controlling the number of electrons that occupy a particular valley, it is possible induce a valley "polarization", which can then be used to transmit/process information. This new degree of freedom behaves mathematically in a similar way to the electron spin in that it acts like additional intrinsic angular momentum of the electron. Electrons can be valley polarized by scattering off a line of defects.

Several recent advances in nano-technology have demonstrated the viability of bio-metallic and bio-semiconductor interfacing, leading to the possibility that future detection systems may be directly interfaced to biological systems (the operator), or alternately, biological systems may be nano-engineered to be detection systems.

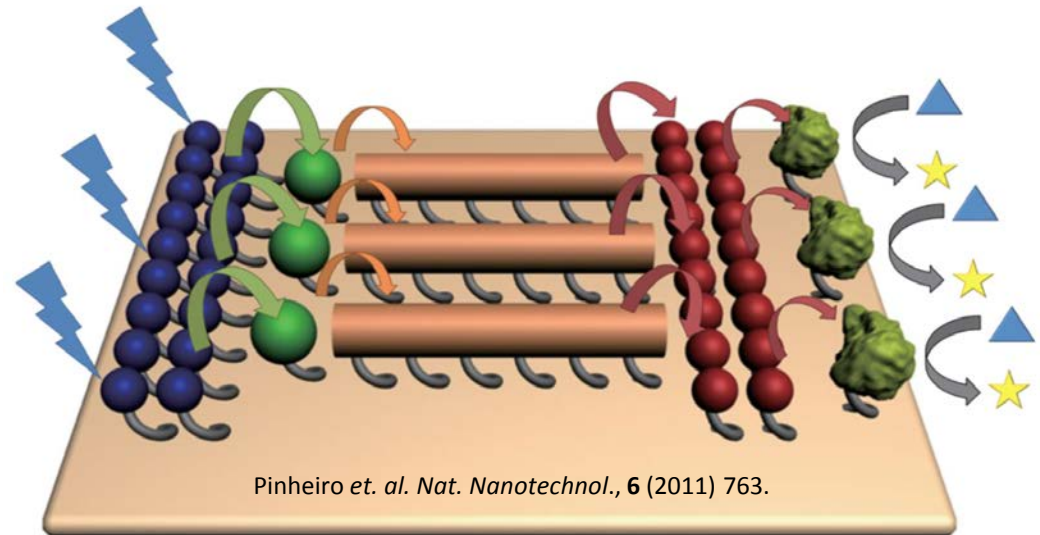
* porosity in III-V compounds, particularly, GaAs, GaP and InP leads to the possibility of animal cell:semiconductor interfacing as in the case of nanostructured Si (Bayliss, et al., "The Culture of Mammalian Cells on Nanostructured Silicon", *Advanced Materials*, Vol. **11**, Issue 4 (1999) pp. 318

* The porous semiconductor serves as both the adhesion substrate for Neurons which act as transducers/receivers. Preliminary work has demonstrated that mammalian cells can be cultured on nanostructured Si that remain viable over time - both in terms of respiration and membrane integrity.



(a) Single strands of DNA consist of a sugar-phosphate backbone decorated with organic bases. A double helix forms when the bases of one strand form hydrogen bonds to complementary bases on another strand. (b), Tanaka *et al.*, *Nature Nanotech.*, **1** (2006) 190, have replaced bases in natural DNA with artificial ones that bind specifically to copper ions (Cu^{2+} , purple spheres) or mercury ions (Hg^{2+} , orange spheres)

Matzczyny, Olesiak-Banska "DNA as scaffolding for nano-photonic structures", *J. Nanophotonics*, **6** (2012) 064505



Pinheiro *et al.* *Nat. Nanotechnol.*, **6** (2011) 763.

Schematic of a DNA-based machine for energy transfer and photonics. The blue, green and red spheres and orange rods represent photonic components that can serve as light-harvesting and energy-transfer materials. The uneven green spheres represent enzyme or membrane complexes that can be used as final energy or electron acceptors. These act as molecular transducer units, where light is transformed into chemical potential, represented by the transformation of substrate (triangles) or into a higher-energy product (stars).

We need better material and to explore other degrees of freedom – until then targeted material engineering (e.g., dimensional reduction) and use single sensing techniques

for more information see

